Master's thesis

NTNU
Norwegian University of Science and Technology
Department of Manufacturing and Civil Engineering

Almar Vreim Brandal

Development of a Modular Polyethylene Pipe Hull and GFRP Rudder System for an Autonomus Surface Vessel

Master's thesis in Mechanical Engineering
Supervisor: Andreas Echtermeyer
August 2021

NTNU
Norwegian University of Science and Technology

Almar Vreim Brandal

Development of a Modular Polyethylene Pipe Hull and GFRP Rudder System for an Autonomus Surface Vessel

Master's thesis in Mechanical Engineering
Supervisor: Andreas Echtermeyer
August 2021

Norwegian University of Science and Technology
Department of Manufacturing and Civil Engineering

NTNU
Norwegian University of
Science and Technology

Abstract

autonomous surface vessels (ASVs)'s are expected to soon be ready to undergo long missions in remote locations in the ocean. These vessels can serve as valuable data acquisition centers for a number of different industries. Energy efficiency and durability are prerequisites for a long term mission of a ASV to be successful. The vessels must also be low cost to be commercially viable at a large scale. Great interest has therefore been dedicated to autonomous sailing vessels, as they require a very small amount of energy for propulsion. The development and production of the hull and rudder system of such a sailing vessels is documented in this master thesis, as part of the Oceanographic Research Craft Autonomous (ORCA) project.

The hull was designed to be made of PE pressure pipes. The prototype hull consists of four separate compartments and can be connected to each other via a novel internal flange bolted connection. A full scale prototype was manufactured and tested. During the waterproof testing it became clear that several of the connections leaked, thus reveling the weakness of the design.

A composite rudder was designed and a functional prototype was produced. The rudder was made using various composite manufacturing techniques, with focus on production efficiency for prototyping. The rudder has a skeg design and is driven by a linear actuator. The rudder was assembled and its basic functionality tested. The rudder system manufactured was functional during testing.

Sammendrag

Det akademiske fagfeltet rundt autonome overflatefartøy er snart klare til å produsere fartøy kapable til lange oppdrag langt til havs. Disse fartøyene kan fungere som data insamlere for en rekke forskjellige industrier. For å håndtere lange oppdrag til havs trenger fartøyene å være energi effektive og sold bygd. I tillegg til dette må farkostene også være billig å produsere for å lykkes i stor skala. Autonome seilings fartøy har fått mye oppmerksomhet i nyere tid grunnet deres lave energibruk. Utviklings og produksjonsprosessen av et skrog og et ror system i et slik autonomt seilingsfartø blir presentert i denne rapporten. Dette prosjektet er en del av et større prosjekt der det autonome overflatefartøyet prototypen Oceanographic Research Craft Autonomous (ORCA) blir utviklet.

Skroget ble designet som en modulær sylinder bestående av PE trykkrør. Skroget har fire seksjoner som er koblet sammen via en intern boltet flens kobling. Et full skala skrog ble produsert og testet. Flere lekkasjer ble funnet I rørkoblingene under en test for å sjekke vantetthet.

Et kompositt ror ble designet og en fungerende prototype ble produsert. Roret ble laget gjennom en rekke forskjellige kompositt fabrikkerings metoder. Fokuset for valg av produksjonsmetode var å bruke metoder som egnet seg for prototyping. Roret ble sammenstilt og testet. Ror systemet fungerte under funksjons testen.

Contents

Figures

Tables

Acronyms

ASV autonomous surface vessel. iii, 1–3, 5, 6, 83

AWJ Abrasive water-jet. 13, 64

CAD computer aided design. 19

CFRP carbon fibre reinforced polymer. xii, 3, 39–41

FEA finite element analysis. xii, xv, 19, 27, 28, 32, 33, 36, 39, 42, 45, 84

FRP fiber reinforced polymer. 11–13

GFRP glass fibre reinforced polymer. xii, 19, 30–33, 35, 39, 66

HAZ Heat Affected Zone. 12, 13, 31

HDPE high density polyethylene. xi, 15, 19, 20, 25

NACA National Advisory Committee for Aeronautics. 5, 38

OD outer diameter. 20

OoA Out of Autoclave. 11

ORCA Oceanographic Research Craft Autonomous. iii, 2–6, 19, 30, 38

PSMC Pipe Sections with Mast Connector. 19, 20, 24

SDR standard dimension ratio. 20, 21, 27–29

SF safety factor. 4, 32, 34, 35, 40

UTS ultimate tensile strength. 16, 17

VARI vacuum assisted resin infusion. 9

VARTM Vacuum assisted resin transfer moulding. vii, 9, 10, 35, 39, 40

WRSC World Robotic Sailing Championship. 2

Chapter 1

Introduction

Data collection is an important part of our rapidly evolving world, and such data collection from the ocean is much needed. Weather and climate change monitoring and prediction, biological observation and preservation are some of the motivating factor for exploring the ocean further. There are many challenges and dangers with having humans permanently stationed on the ocean to collect data. This project evolved with the goal to bypass theses challenges, as a wind propelled autonomous surface vessels ASV can collect data reliably and risk free.

Autonomous vehicles has bean developed and used in a number of different industries. From NASA's Perseverance on mars, to autonomous trucks and delivery systems. The benefits of these autonomous vehicles are many as they can go and operate where humans can not and as long as they have power they can operate continuously. This same technology of long term autonomous missions, delivering data and surviving harsh environments, can be off great benefit in our oceans.

1.1 The State-of-the Art in Autonomus Sailing Vessels

Autonomous sailing vessels are a category of ASV, where wind power is the only source of propulsion. Earlier research was mainly focused on short-range ASVs powered by electrical or combustion engines [1]. In recent year some focus has shifted on longer missions further off shore. The new focus on longer missions demands a power efficiency of the ASV that traditional engine powered vessels can not offer. This has resulted in a resent interest in autonomous sailing vessels with key characteristics Stelzer and Jafarmadar [1] as follows:

- Wind is the only source of propulsion.
- It is not remotely controlled; the entire control system is on board.
- It is completely energy self-sufficient.

In 2006 Neal [2] published a study that showed the feasibility of a low-cost and low-complexity autonomous sailing vessel. The 1.5m long ASV managed to hold station in a lot of different wind and wave conditions. The vessel struggled in rougher seas however, and the author suggests a 3m long boat as a suitable

length in an open ocean scenario.

In 2019 Silva *et al.* [3] conducted a state of the art survey of rigid wing sailboats, with a focus on autonomous sailing vessels. This article compared many different autonomous sailing vessels from both the commercial and the academic sectors from an early prototype in 2001 up to the commercial ASV Saildrone in 2018. There have been several robotic sailing competitions in resent year that has attract media attention and raised research funds to the autonomous sailing field [1]. Most prominently of these are the Microtransat; which is a transatlantic race for fully automated sailing vessels, SailBot; a multi-event competition with races, endurance testes, and navigation tests, and the World Robotic Sailing Championship (WRSC). the WRSC changes its specific rules every year to reflect recent scientific developments.

Several hull designs have been presented for a wind propelled ASV in literature. Some of the key characteristics that have been found important in the hull design is light weight and the ability to self right in the event of capsizing [3].

The actuation of the sail and rudder are the two main power draws in a wind propelled ASV. The rudder actuation being reported in one case to consume 75% of the overall power consummation [4]. Making these two systems power efficient is of great importance and making use of worm gears that minimize power consumption when the rudder or wing is standing still has been positive. Many ASVs have incorporated solar panels to extend mission time, such as the SailBuoy, a Norwegian wind propelled semi autonomous surface vessel that was the first of its kind to complete an Atlantic crossing [3]. The SailBuoy is not fully autonomous, but navigates autonomously from fixed way-points.

1.2 Standing Challanges in Autonomus Sailing Vessels

Many of the robotic sailing competitions and earlier research focused on the ASVs speed and maneuverability. Vessel robustness and reliability is cited as one of the fields next challenges [3].

As the field of ASVs is one of prototyping in academia, it is important to experiment with fast and cheap manufacturing techniques to be able to iterate on the designs with satisfactory progress. These fast and novel manufacturing processes has not been a focus of the ASV literature as many research groups either modifies existing sailing vessels or sticks to conventional fabrication methods of glass fiber reinforced polymer construction.

1.3 the ORCA Project

This master thesis is a contribution to the Oceanographic Research Craft Autonomous ORCA project. A project founded by A. Echtermeyer and the Department of Mechanical and Industrial Engineering at the Norwegian University of Science

and Technology. The projects objective is to develop a low-cost small autonomous vessel that can be out at sea for several years. The vessel should be able to perform scientific measurements and transmit the data in real time. The project focus is on the design of such a vessel, not the instrumentation. The eventual goal is to design ASV that can be mass produced and be used as a platform for many different oceanography projects.

Figure 1.1: ORCA project logo.

The project started in 2019 and several people have been involved since then. Gården Rovik [5] wrote a project thesis exploring various overall design solutions for an ASV. Dyrseth [6] wrote both a project thesis and master thesis on the design and construction of a carbon fiber reinforced polymer rigid wing sail during 2019 and 2020. In 2021 L. Digerud worked on the development of a hydrogenerator as an additional energy source for the ASV.

In the fall of 2020 Gauden [7] wrote a project thesis about a new actuation and rigid wing sail system. During this time the author wrote a project thesis about the development of the hull and rudder system of the ASV Brandal [8]. That project thesis is the foundation of this master thesis and relevant results will be presented in Section 1.4, Section 4.1.1, and Section 4.2.1.

During the spring of 2021 the first prototype of the ORCA project was finished and tested by S. Gauden and the author, shown in figure 1.2. The prototype named CAT was a converted 3 meter long catamaran with the CFRP sail Dyrseth [6] designed and a rudder designed by the author.

Figure 1.2: CAT during first field test

1.4 Project Foundation

The ORCA vessel was designed according to a hierarchy of design goals, Table 1.1, and requirements, Table 1.2, presented bellow.

Table 1.1: Vessel hierarchy of design goals.

1	Durability
2	Cost
3	Ease of manufacturing
4	Ease of repair
5	Stability
6	Manoeuvrability
7	Environmental friendliness
8	Speed
9	Seaworthiness/Certification

For the structural integrity of the hull it was decided that it needed to withstand a bending test with a payload of $200kg$ with a safety factor (SF) of 2.

The critical load case for the rudder was derived by taking the minimum service speed, which is assumed to be close to the vessels maximum speed, and placing the rudder geometry perpendicularly on the water stream. The fluid force

Table 1.2: Vessel design requirements.

Design aspect	**Requirement**
Approximate vessel size	$3\,m$
Minimum service speed	$1.5\,\frac{m}{s}$
Energy consumption	Less than or equal to energy generation
Maximum apparent wind speed	$20\,\frac{m}{s}$
Lifetime, supervised	25 years
Lifetime, unsupervised	1 year
Minimum carrying capacity	$200\,kg$
Operational temperature range	-20^oC - 40^oC

experienced by the rudder would then be

$$F_d = \frac{1}{2}\rho v^2 A C_d \tag{1.1}$$

where c_d is the coefficient of drag and for an approximate flat surface is equal to 1.28. Having the fluid flow perpendicular too the rudder is very unlikely during normal operations, but could occur during strong currents. The dimensions and National Advisory Committee for Aeronautics (NACA) profile of the rudder was decided in the authors project thesis [8].

1.5 Objective

This thesis tackles the design of both the hull and the rudder system of the ORCA project and therefore has two research objectives, one for each system. The objective of the hull section is to explore the possibility of using polyethylene pipes to make a modular hull for an ASV that meets the design goals bellow, Table 1.3. The objective of the rudder section is to produce a rudder system that meets the same design goals as the hull while implementing efficient and fast prototyping manufacturing processes.

1	Robust
2	Reliable
3	Low cost
4	Low manufacturing time
5	Assemble/disassemble easily
6	Low weight
7	User friendly

Table 1.3: Hull and rudder system objectives.

1.6 Methods Used

To achieve these objectives, a prototype design has been developed and manufactured. The hull has gone through system tests related to robustness and ease of assembly and the rudder has been tested to check for basic functionality.

1.7 Thesis Structure

Chapter 1	An introduction and brief overview of the state of the art of ASVs. Presentation of the ORCA project and the thesis objective.
Chapter 2	Relevant theory concerning composite modeling and manufactoring.
Chapter 3	Relevant theory concerning thermoplastic manufacturing and welding as well as O-ring theory.
Chapter 4	The development process is documented and discussed. .
Chapter 5	The manufactoring process.
Chapter 6	The experimental setup and results.
Chapter 7	Discussion of experimental results, the design process and the manufacturing process.
Chapter 8	Summarizes the thesis and poses conclusions.

Table 1.4: Thesis structure

1.8 Thesis Limitations

The main focus while working on this thesis, as for the ORCA project, has been to produce a functional prototype. The limited intent was to show proof-of-concept.

The practical work of building the vessel proved to be very time consuming and has come at the expense of detailed analysis, and simulation work. The complete ORCA prototype then, could not be finished in time, which also prevented a full system test of the ASV.

This thesis is focused on the mechanical and structural sides of the vessel and does not go into detail about electronics or vessel control. Further more, a proper fatigue study has not been done for any of the components designed, as was deemed unnecessary to show proof of concept.

Chapter 2

Theory on Composites and Composites Manufacturing

2.1 Laminate Theory

Laminate theory is a mathematical model used when modeling and understanding composite materials. It provides the strain and stress distribution for each ply from the material properties as well as for the stacking sequence [9]. From this an appropriate failure criteria can be imposed to predict the parts failure. In this thesis laminate theory was used during the modeling of the rudder, Section 4.2, and skeg, Section 4.3.

2.1.1 The ABBD matrix and desired material properties

$$\begin{Bmatrix} N \\ \hline M \end{Bmatrix} = \left[\begin{array}{c|c} A & B \\ \hline B & D \end{array}\right] \begin{Bmatrix} \varepsilon^0 \\ \hline \kappa \end{Bmatrix}$$

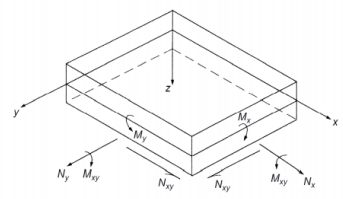

$$\begin{bmatrix} N_x \\ N_y \\ N_{xy} \end{bmatrix} = \begin{bmatrix} A_{11} & A_{12} & A_{13} \\ A_{21} & A_{22} & A_{23} \\ A_{31} & A_{32} & A_{33} \end{bmatrix} \begin{bmatrix} \varepsilon^\circ{}_x \\ \varepsilon^\circ{}_y \\ \varepsilon^\circ{}_{xy} \end{bmatrix} + \begin{bmatrix} B_{11} & B_{12} & B_{13} \\ B_{21} & B_{22} & B_{23} \\ B_{31} & B_{32} & B_{33} \end{bmatrix} \begin{bmatrix} \kappa_x \\ \kappa_y \\ \kappa_{xy} \end{bmatrix}$$

$$\begin{bmatrix} M_x \\ M_y \\ M_{xy} \end{bmatrix} = \begin{bmatrix} B_{11} & B_{12} & B_{13} \\ B_{21} & B_{22} & B_{23} \\ B_{31} & B_{32} & B_{33} \end{bmatrix} \begin{bmatrix} \varepsilon^\circ{}_x \\ \varepsilon^\circ{}_y \\ \varepsilon^\circ{}_{xy} \end{bmatrix} + \begin{bmatrix} D_{11} & D_{12} & D_{13} \\ D_{21} & D_{22} & D_{23} \\ D_{31} & D_{32} & D_{33} \end{bmatrix} \begin{bmatrix} \kappa_x \\ \kappa_y \\ \kappa_{xy} \end{bmatrix}$$

Figure 2.1: The equation describing the relationship between section forces and moments and mid-surface stress and curvature using the ABBD matrix.

The **ABBD**-matrix in Figure 2.1 contains the material properties of the laminate in different orientations. **A** considers the tension-compression effects of longitudinal and transverse loading, matrix **D** considers the effects of bending moments, while matrix **B** couples the effects of both types of loading [9]. By manipulating the lamina layup orientation and stacking sequence, specific material properties can be engineered. This material response to layup is easily understood by looking at the **ABBD**-matrix.

In a balanced layup there are an equal amount of lamina with 1-direction of $+\theta$ as there is with $-\theta$. In such a layup, section-normal forces is decoupled from shear strain and section-shear forces from normal strain. This is shown in the A-matrix as $A_{13} = A_{23} = 0$.

Symmetry in composite layup refers to mirror symmetry about the mid-plane of the composite stack. For a stack to have a symmetric lamina orientation, layup sequence and thickness must be symmetric about the mid-plane. This result in **B**-matrix equal to **0** and eliminates bending-stretching coupling. This happens as the contributions of the lamina above the mid-plane counteracts the contributions below. Such a symmetric laminate will therefore not twist when subjected to in plane forces. Neither will its mid-plane elongate during moment forces [10]. Thus it is desirable with a symmetrical layup. Further more, this layup does not warp during curing and will retain high geometrical accuracy.

2.1.2 Laminate failure criteria

Laminate failure in composites is usually defined as first ply failure. This is highly dependent on lamina direction as the lamina are orthotropic. Two of the failure criteria Abaqus provides in its FE analyses is Tsai-Wu and Tsai-Hill, shown in figure 2.2. The World Wide Failure Exercise[11] shows that the Tsai-Wu criteria had the best co-relation with experimental results. The two failure criteria preform similarly in tension, but Tsai-Hill is a bit more conservative in compression.

Tsai-Hill was chosen as failure criteria in this thesis because of the conservative compression approach as well as to achieve a consistent failure criteria for the ORCA project as a whole.

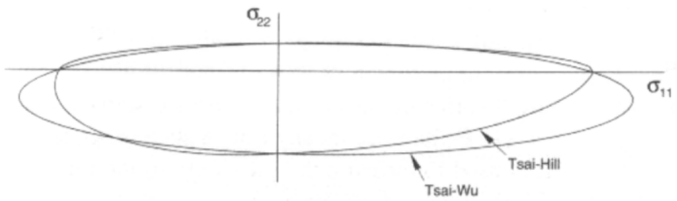

Figure 2.2: Comparison of the Tsai-Hill and Tsai-Wu criteria.[11]

The Tsai-hill index is used to describe the level of stress in a lamina relative to failure. An index, I_F^{T-H}, greater than 1 indicates failure.

The failure theories discussed above are based on assumptions not applicable near free edges, holes, and fiber endings [9]. In these areas the through-thickness-shear-stress, that these theories assume to be zero, dramatically increases, and the in-plane-stresses decreases. In these ares different failure theories need to be applied. [9].

2.2 Vacuum Assisted Resin Transfer Moulding

VARTM, also called vacuum assisted resin infusion (VARI), is a composite manufacturing process. Vacuum has a dual purpose in the process as it compacts the fibers into the mold with an even pressure and creates a pressure difference that sucks the resin into the fibers. A schematic of the process with all the necessary equipment is shown in figure 2.3. This illustration explaines the basics of how a standard VARTM is done. For further detailed description of the process K.-T. Hsiao and D. Heider, 'Vacuum assisted resin transfer molding (vartm) in polymer matrix composites,' in *Manufacturing techniques for polymer matrix composites (PMCs)*, Elsevier, 2012, pp. 310–347, chapter 10.

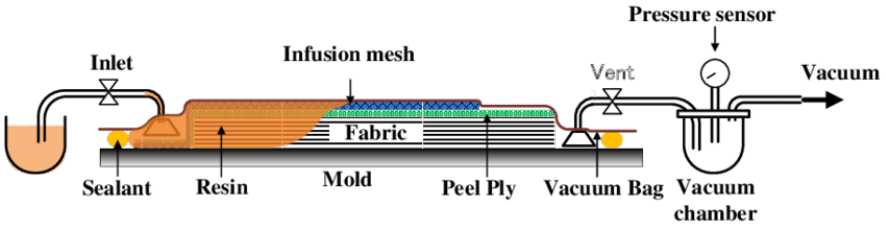

Figure 2.3: A schematic diagram of VARTM process.[13]

2.2.1 VARTM Processes Variant: Flow Mesh

Over the years many innovations and variations of the standard VARTM process have taken place. Flow mesh, in figure 2.3 called infusion mesh, used to increase intra-tow flow rates, was found to also reduce thickness variance in a study by Van Oosterom *et al.* [14]. The result of their tests showed a reduction of thickness difference in the test sample from 5% to 0.3%. This happens as the flow mesh rapidly distributes the pressure differences in the post-filling phase.

The flow rate of the resin will impact the void content in the part. Voids can form both if the resin flow is too slow or to fast, as shown in figure 2.4. With the use of an infusion mesh in the VARTM process, macro voids from low flow rates can be avoided. [14].
High flow front advancement has been shown to trap micro bobbles in fiber tows as the velocity difference between the intra-tow and inter-tow resin flow become too great [15],[14]. An optimum flow rate will be when the intra-tow and inter-tow flow rates are equal. This will minimize the occurrence of macro and micro voids.

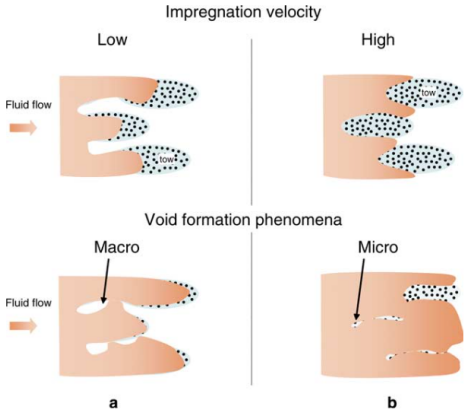

Figure 2.4: Impregnation mechanisms in a dual-scale porous medium: (a) formation of macro-voids due to capillary forces (low resin velocity); (b) formation of micro-voids due to viscous forces (high resin velocity). [15]

To reduce intra-tow flow rates, the resin permeability of the flow medium or the pressure difference between inlet and outlet, can be reduced.

Ruiz *et al.* [15] proposes an optimization algorithm to ensure the right resin flow.

2.2.2 VARTM Processes Variant: Mouldless

The mouldless VARTM process is a relatively new manufacturing process used for prototyping and low quantity production runs. It was first described in Maley [16] where it was used to manufacture an H-frame for an Unmanned Aerial Vehicle prototype. As shown in figure 2.5, the foam core of the composite is used instead off a mould, as fabric and other components of the VARTM is wrapped around the foam core.

It is an advantages to use a mouldless process when producing small batches, as the machining required to make a mould can be eliminated. On the other hand the surface finish will not be as good as that of a VARTM in a female mould. In Maley [16] the author also stated the warping during curing and post curing was a bigger problem compared to normal VARTM. This was caused by the lower stiffness of foam compared to normal moulding materials. A proposed solution for this was to implement a support structure inside the foam to help with rigidity.

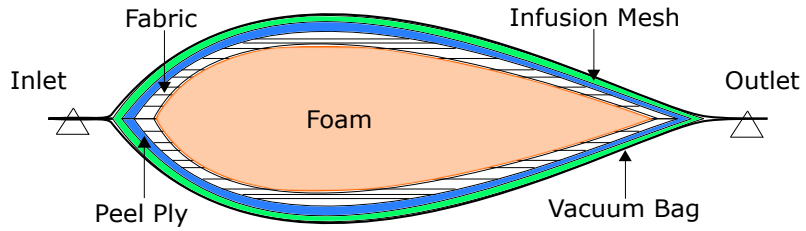

Figure 2.5: A schematic diagram of the mouldless VARTM process.

2.3 Out of Autoclave Prepreg Manufactoring

The Out of Autoclave (OoA) prepreg manufacturing method uses preimpregnated fibers that are design to cure with the use of vacuum and an oven. This is opposed to the autoclave method were the composite part is cured in a pressure oven at elevated pressures. The prepreg fibers are cut and placed into the mould by hand. A vacuum is drawn around the mould and the part is placed in the oven. OoA prepreg manufacturing can achieve material properties similar to that of an autoclave, but with a reduced cost and the added design flexibility of being able to produce large parts that can not fit in an autoclave [17].

2.4 Filament Winding

Filament winding is a composite manufacturing method were filament, impregnated with resin, is wound around a mandrel. Filament winding is typically used in the manufacturing of pressure vessels, pipes and other cylindrical and conical objects. The process can use both prepreg and wet filament. A benefit to filament winding is the ease of which specific material properties can be given to the part by changing the winding pattern [18]. A hoop winding would improve strength against buckling, while helical winding, with a low angle, improves bending strength.

The benefits of the filament winding process compared to hand lay-up are its high production rates once set up, repeatability, and quality stability. Disadvantages to the production method are the high initial set up time, and constraints on placement angle relative to mandrel shaft [19].

2.5 Post Processing of Fiber Reinforced Polymer Composite Laminates

Cutting and machining of fiber reinforced polymer (FRP) are required in nearly all production methods to trim edges and to make certain geometries such as

holes. When cutting the composite material, edge defects will occur due to the interaction between the tool and the inhomogeneous mixture of matrix and fibers. The components of the composite material respond differently to the machining tool depending on factors such as fiber volume fraction, fiber orientation, matrix elasticity and more [20]. The high tool wear during machining of composites is also a problem, as conventional tools are worn down by the carbon, aramid, or glass fibers.

Komanduri *et al.* [21] studied the effect of fiber direction relative to tool orientation during machining. When the fiber direction was $+10^o$ in the $+\theta$ direction ($+\theta$ gives the angle counterclockwise from the machined surface), the fibers bent underneath the tool and delamination occurred. When the fibers were oriented -10^o they broke in tension, resulting in much fewer edge defects. This shows that small variables, that may be hard to control, in post processing may have great impact on the end result.

During conventional drilling two distinct delamination processes take place. The top layers of the composite peel-up at the entrance of the tool by the axial force created by the slope of the drill flute [22]. The second delamination process happens as the drill tool reaches the end of the material. As the material left underneath the tool decreases so does also its bending strength. The last plies is pushed out and break away before the drill has completely penetrated the composite.

To minimize delamination during conventional drilling, higher cutting speeds, lower feed rates, and harder tool materials is preferred. Applied pressure around the area to be drilled, "a hold" on the top and bottom surface, will also help reduce delamination since this will increase bending strength while machining.

To combat rapid tool wear and to ensure accurate cuts, advanced machining methods such as laser cutting and water jet cutting can be implemented. These are both non-contact machining methods and does not degrade the tool when cutting composites.
Laser cutting works by hitting the material with a concentrated laser that melts and vaporizes it. Komanduri *et al.* [21] describes three different material defect that occur during laser cutting of FRP as shown in figure 2.6. These defects are the constituent parts of the Heat Affected Zone (HAZ) which is the area considered damaged from the cutting process.

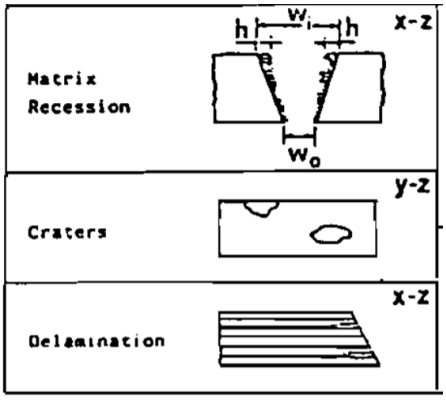

Figure 2.6: Laser cutting defects [21]

The first is a matrix recession that happens as the matrix has a lower degradation and evaporation temperature than the fibers. The second is crater formation along the cutting direction and the third is delamination.

The quality of the laser cut depends only upon the interaction time between the material and the laser. Less interaction time means less thermal energy transfer and a smaller HAZ. To keep the cutting speed high is crucial, thus laser cutting is limited to cutting relatively thin FRP parts.

Abrasive water-jet (AWJ) cutting is similar to laser cutting, but with some different advantages and challenges. AWJ cutting cuts by erosion. The water in the water-jet also acts as a coolant and reduces the HAZ [23]. The method can therefore cut thicker work pieces than laser cutting.

Even though abrasive water-jet cutting can operate at high speeds, delamination tend to occur with a high feed rate. To avoid excessive delamination, a maximum speed of $1m/min$ is recommended. This is still nearly four times faster than traditional methods and makes AWJ the preferred cutting method for many applications [23].

On initial penetration the water-jet tends to cause delamination similar to that of a drill. It is therefore recommended to make the initial cut in waste material.

Chapter 3

Thermoplastic Coupling and O-ring theory

3.1 High-Density Polyethylene Pipe Construction and Properties

A HDPE pipe was to be used as the hull for the ORCA prototype. These pipes are made in a hot plastic extrusion process, where polymer pellets are melted and extruded through a die as shown in figure 3.2. The pipe is extruded into a cold water bath which cools the polymer rapidly to retain its shape [24]. This process induces residual stresses in the material in two stages.

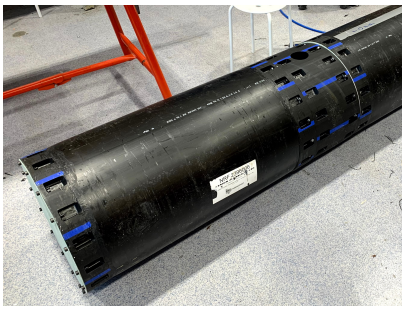

Figure 3.1: The extruded HDPE pipe used for the ORCA project

Firstly, flow stresses, as the material is forced through the die. Secondly, thermal stresses, as the pipe is rapidly cooled down in the cooling tank. The flow stress is a consequence of incomplete relaxation of the material before freezing and the thermal stress occur as the outer walls cool faster than the inner walls of the tube during cooling [24]. This results in the outer wall being in compression and the inner wall being in tension.

These residual hoop stresses are released at the edges when a cut is made and results in a contraction of the outer diameter of the pipe. This dimensional change can be pretty substantial as HDPE is a ductile material and deforms easily.

The residual hoop stress is one of the main driving factors of slow crack growth in HDPE pipes, and they are one of the determining factors in lifetime expectancy. Even with this these internal hoop stresses modern PE blends are usually guarantied a lifetime of over 50 years [25] so this is not relevant for the ORCA project.

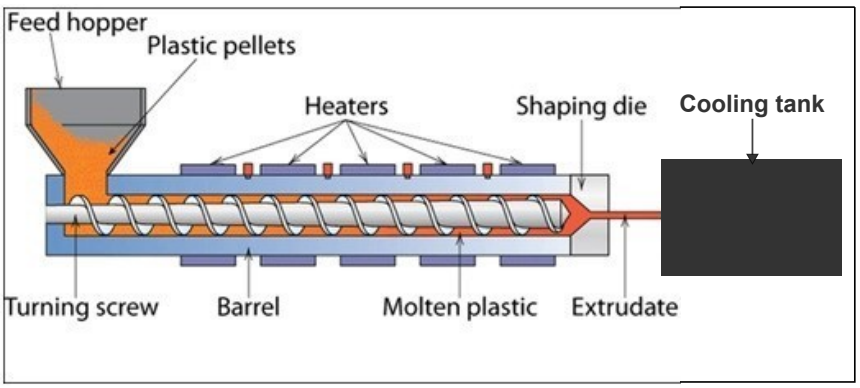

Figure 3.2: A schematic of the polymer extrusion process

3.2 Thermoplastic Welding

Welding is a common way of joining thermoplastics together as they experience little, too no, degradation from being remelted. It creates a permanent, water and gas tight, joint. As with metal welding there are many different variations of the process, with different ways to control process parameters such as heat, pressure and atmosphere content. The two processes that were considered for the ORCA project were mirror welding and extrusion welding.

3.2.1 Mirror Welding

Mirror welding is a butt welding process. The ends of the two tubes that are to be joined are heated by a thin metal plate: the mirror. The mirror is then removed and the two tubes are pressed together quickly, while their edges are still molten. The weld is then cooled, which is often done in room temperature.

Belaziz Azzeddine [26] shows that mirror welding does not reduce the ultimate tensile strength (UTS) of the PE. In fact it increases by a small percentage. However, the weld does experience a slight stiffening and become less ductile. These great joint properties, as well as the ease of use and speed of operation, is the reason mirror welding is the industry standard for thermoplastic pipes. The main drawback for this method is the heavy and large tool that is needed (mirror, electric power source for resistance heating of mirror and pressing tool to press the tube ends together), making it hard to transport and to fit the tool at tight spaces. The method is not used for angled or curved welds.

3.2.2 Extrusion Welding

In extrusion welding a weld groove is cut out of the tubes that are to be welded and a weld rod is pressed into the groove while heated until melting, as shown in figure 3.3. The welding rod can be heated by different means, but hot gas and electric heating is common. The weld groove can ether be cut in a V pattern; on

one side of the wall, or in an X pattern; on both sides. In the welding of pipes only the V groove is feasible unless the pipe is very big and can fit a human with extrusion welding equipment.

The extrusion welder is usually a small portable device operated by a human; more flexible to use compared to the mirror welding, which are big and heavy. Extrusion welding is not limited to butt welding, and just like a conventional metal welder, it can be used to weld many other geometries. However, extrusion welding does not have the same weld factor, (f_w), as mirror welding, and it is more time-consuming and thus expensive.

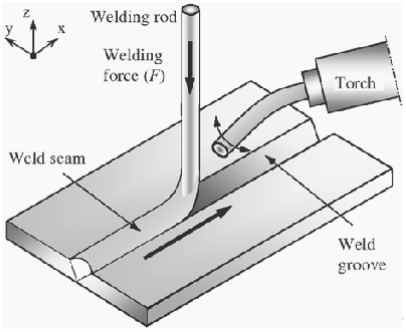

Figure 3.3: A schematic of a extrusion welding process called hot gass weldning [27]

Weld factor describes the comparative strength of the weld to the base material and is defined as

$$f_w = \frac{\sigma_{weld}}{\sigma_{base}}, \tag{3.1}$$

where σ_{weld} and σ_{base} are the UTS of the weld and base material, respectively [27]. In mirror welding f_w can be above 1 and are typically never weaker than the base material, but for extrusion welding the best f_w that has been achieved with a V-groove is 0.9 [26], [27].

3.3 O-ring Theory and Standards

O-rings are the most frequently used type of gasket seals. It is shaped like a torus and has a circular cross section. The internal diameter of the torus is called d_1 and the diameter of the cross section is d_2. The sealing effect of an O-ring comes from being compressed between two components. O-ring seals can be used to make a fluid and/or a gas tight seal. There are two main types of O-ring seals; static and dynamic. The type of seal that was used in the ORCA project was static face seal. For a seal to be successful, the rigid mounting must provide even and constant pressure on the ring.

3.3.1 O-ring housing

The O-ring housing is a gland in one of the two components that compress to make the seal as shown in figure 3.4. The housing must be wider then the O-ring cross sectional diameter, but also have smaller height. This ensures that the O-ring is compressed and a seal is formed. The total cross sectional area of the

housing must be greater then that of the O-ring to prevent O-ring extrusion. O-ring extrusion happens when the O-ring is forced outside of its housing and is compressed directly between the seal faces. This leads to O-ring rupture.

At high external or internal pressures the O-ring can be forced out of the O-ring housing and O-ring extrusion occur. To prevent this, anti-extrusion rings can be installed in the housing on either side of the O-ring.

The O-ring housing dimensions for the appropriate O-ring cross sectional diameter and inner diameter, in this thesis, was extracted from ISO3601-2 *Fluid power systems – O-rings – Part 2: Housing dimensions for general applications* [28].

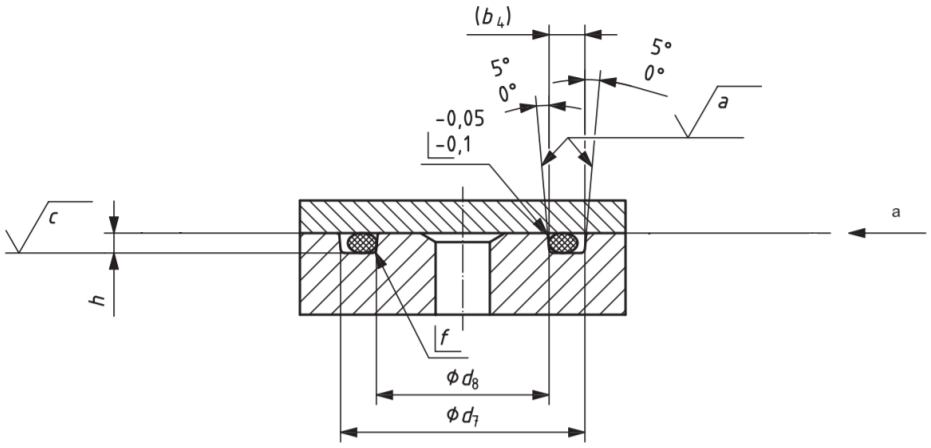

Figure 3.4: Illustration of housing for face seal with external pressure [28].
a,c = surface roughness
d_8 = Internal diameter of housing
d_7 = External diameter of housing
f = housing radius
b_4 = housing width
h = housing height

3.3.2 O-ring Material Theory

Material selection of O-rings are dependent upon the chemical makeup of the environment of the seal, application temperature, pressure, size and cost. Most of the available materials are vulcanized thermosets, but there are a few thermoplastics as well.

Chapter 4

Development

Both the hull and rudder system started its development last year with the work done on the authors project thesis Brandal [8]. The designs were developed further and prepared for manufacturing and assembly. Both systems had rough hand calculations done and were later modeled with computer aided design (CAD) software, *SolidWorks*, and analyzed using FEA in *Abaqus* and *SolidWorks*.

4.1 Development of the Hull

4.1.1 Foundation

The project thesis Brandal [8] found that two different mono hull configurations were promising for the ORCA project. The two hull shapes were a conventional mono hull made by GFRP and a modular design made up of HDPE pipes as shown in figure 4.1. The pipe hull was named Pipe Sections with Mast Connector (PSMC) as it featured a separate hull segment for the mast connection. In that thesis the author was not able to conclude which of the two designs was the best fit for the project.

Both hull designs were deemed to be durable but the PSMC was expected to have a slightly lower cost and build complexity during prototyping than the conventional hull. The PSMC hull would also have the benefit of being modular, so different sterns and bows could be made for specific missions. The conventional

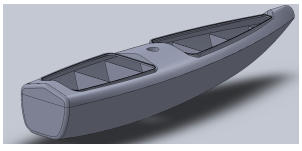

(a) A conventional mono hull design.

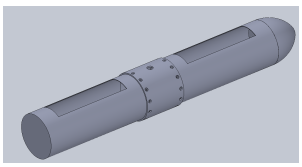

(b) The PSMC design shown as first imagined during the project thesis.

Figure 4.1: The two designed that scored the best in the project thesis [8]

hull would on the other hand have the benefit of being easily optimized and have higher manoeuvrability and hydro-static stability.

During the initial stages of the master project it was decided to go with the PSMC hull as this was a novel concept. The outer diameter (OD) of the pipes were set to 500mm. There would be four modular compartments in the hull design. From stern to bow the compartments would be: rudder compartment, stern storage, mast connection, and bow storage. This design resulted in three pipe connections and two end cap seals having to be designed.

Thermoplastic pipes would be ordered and machined such that they could be fitted together into a 3m long hull.

4.1.2 Material selection

The two materials that are used for pressure pipes in industry are PVC and PE. PVC has good material properties and can be glued. on the other hand it becomes brittle in the lower bound of the required temperature range, -20^{o}C, and was therefore rejected.

PE is comparatively a very ductile material and therefore has great impact strength. It is also able to function in the specified temperature range. PE as a height coefficient of thermal expansion which is in some cases nearly double that of PVC.

The HDPE grade most commonly used in industry pressure pipes is PE 100 and was therefore the material chosen. The PE-grade system is a measure for the material density and determines the strength properties, higher number give a higher strain hardening modulus.

The material is further compounded with additives which increases its resistance to UV degradation.

A full table of the material properties of PE 100 is given in the appendix **??**

4.1.3 Wall Thickness

Apart from the PE-grade, the wall thickness of the pipe is the variable that determines strength and also will influence vessel weight. PE pipes are supplied in standard dimension ratio (SDR), and a wall thickness that matched one of the standard dimensions was necessary. SDR and the corresponding wall thickness and weight for the pipe with OD $=$ 500mm is shown in table 4.1.

With an estimation of component weight, maximum carry capacity, and knowing the density of the HDPE, it was possible to calculate a bending criteria for the vessel. This was modeled as a simply supported beam with a vertical load in the middle, representing the total weight of the vessel. This was to mirror the assumed worst case scenario, as the vessel is suspended on two ocean waves, $3m$ apart. The calculated bending stress and deflection are also given for the different evaluated wall thicknesses in table 4.1, annotated as σ and u, respectively.

SDR	t [mm]	m [kg]	σ [MPa]	u [mm]
22	22.8	98	1.5	4.0
26	19.1	83	1.6	4.4
33	15.3	67	1.9	5.2
41	12.3	54	2.2	6.1

Table 4.1: Stress calculation of PE pipe. t is wall thickness, m is hull weight, σ is max stress, and u is max deflection.

As the yield strength of PE 100 is $23MPa$, and maximum bending stress and deflection for the thinnest pipe was only $2.2MPa$ and $6.1mm$ respectively, even the thinnest pipe would be suitable by this requirement alone.

A hull with lower wall thickness, however, could be expected to deform due to thermal expansion and more easily ruptured on impact. Due to these last selection criteria, two independent pipe manufacturers, Wavin and GPA, recommended not using a lower SDR than 26. This advice was taken into account, and a wall thickness of $19.1mm$ was decided.

4.1.4 Plastic Inserts

The hull was designed to have threaded inserts as connection points to external and internal structures. These threaded inserts had to be of a corrosion resistant material and have sufficient pull out strength. The benefits of having threaded inserts was the possibility of having bolt connections without needing to drill a hole in the hull, thus preventing potential leakage points. An insert vs direct threading in the PE-material is stronger and more durable with regard to repeated use.

The chosen inserts were blind self-tapping inserts in a SS316 alloy from Technifast [29], seen in figure 4.2.

Figure 4.2: The blind self-tapping inserts from [29]

The chosen inserts were in M8 size for external structures, and M6 for internal structures. A pull out test was devised to determine the pull out strength of the

inserts. This was done for the M8 inserts only, as these were expected to experience significant loads.

Experimental Setup and Method

The pull out strength of the M8 insert was determined by measuring the pull out force required with a load cell. The M8 insert was tapped into a PE100 pipe with a wall thickness of 17mm. As the length of the insert was 15mm this ensured full contact of every thread. The PE pipe was then secured to a rigid surface and a load cell was screwed into the insert. A moment arm over a guiding platformed was connected to the load cell and weights were fastened to the other side of the moment arm to increase pull out force. The experimental setup is pictured in figure 4.3.

Figure 4.3: Experimental rig. With moment arm and load cell conected to the PE pipe.

As the pull out strength of inserts varies with the pilot hole, multiple pilot holes were tested.

Results

The pull out strength of the M8 inserts are shown in table 4.2. The strength increases with decreasing pilot hole. Since there were fairly large deformations around the insert with the pilot hole of 10mm, the slightly larger pilot hole of 10.3mm was chosen as standard for this project. It had almost the same pull out strength but with much smaller deformations at insertion.

Pilot hole, D_p [mm]	10	10.3	10.6	11
Pull out force, N	6023	5945	5672	4462

Table 4.2: Test result from pull out test.

4.1.5 Internal Storage Trays

To carry batteries, control unit, motors, gears and data collection equipment, a modular storage system was needed for the hull. Consequently trays where designed for the inside of the pipe hull. A benefit of the tray design is the ease of modification as new or modified components can be placed on a tray, and then easily installed into the vessel.

The systems needed a basic guiding profile to fix the tray in the hull, for stability, and the actual tray to slide in place between the profiles. Extruded aluminium profiles were chosen as guiding profiles. These were bolted to the hull with M6 inserts. An early prototype of the system is shown in figure 4.4.

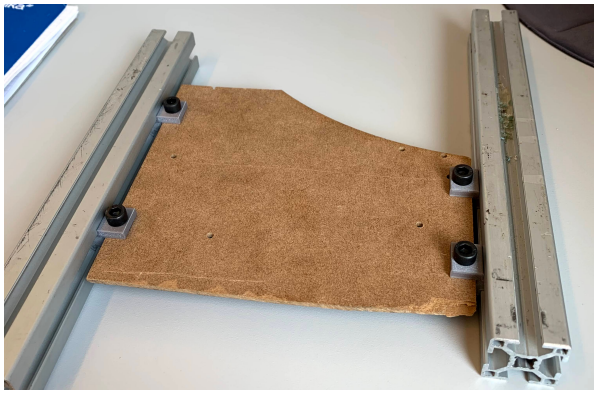

Figure 4.4: Early prototype of Storage tray concept.

Plastic glide connectors were 3D printed to connect the trays to the aluminium profiles. 3D printing was also used to make plastic supports for the aluminium profiles. These plastic supports ensured that the aluminium profiles were level when bolted to the hull. Figure 4.5 shows how the plastic supports connect the two aluminium profiles which aligns them to the holes during installation.

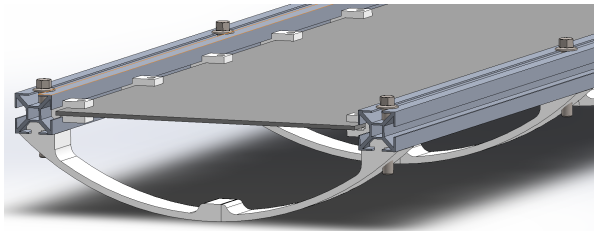

Figure 4.5: Solidworks model of the storage tray assembly.

4.1.6 Buoyancy

A buoyancy study was done to find the waterline of the hull. The waterline can be used to determine drag generated from the hull. On conventional vessels the

waterline also determines the vessels stability, but as the pipe hull has a round cross section this effect is negligible. The mass used for the vessel was the mass estimated in section 4.1.3 with SDR26 pipes and maximum carrying capacity. The Volume of the hull under water was 63%. This equates to the water line being 53*mm* above the midpoint of the pipes.

4.1.7 Exploration of Hull Connections

A critical part of the PSMC hull concept was the pipe connections. They had to be designed in a way that met the system objectives 1.3. Of particular importance were connection strength, water tightness, and ease of assembly/disassembly. Welding the pipes together would have been an easy solution, but this did not seem to mesh well with the intention of a modular system that could be disassembled.

Three different pipe connections were considered during the design process.

Internal Sliding Pipe Connection

The internal sliding pipe connection is based on a common principal used on fittings for smaller pipe diameters. On this construction a pipe, with an outer diameter matching that of the inner diameter of the main pipe, is welded on to make the male part of the connection. The internal pipe is fitted with O-rings in the O-ring housings and slid in the female connection, shown in figure 4.6. The whole assembly is then fastened with bolts into a threaded insert.

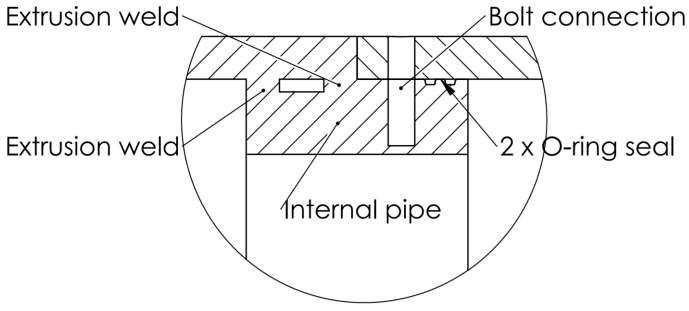

Figure 4.6: A schematic of the internal sliding pipe connection

This connection method was attractive as it resulted in only the bolt heads being proud of the pipe diameter and contributing to drag.

It was however deemed difficult to manufacture as it required internal extrusion welding to fasten the inner pipe. To achieve a pressure fit between the male and female part, with the necessary tolerances to result in a watertight construction, seemed close to impossible. The O-ring had a tendency to get extruded trough the bolt hole of the female connection during prototyping as shown in figure 4.7.

This was solved by chamfering the inside of the female bolt hole, which added complexity and manufacturing time.
In a conversation with a HDPE pipe supplier, Multi Plast, it was said that the shrinkage caused by the released residual stress in the pipe edges would cause the pipe diameter to shrink between 3-8 mm for a pipe with OD500, section 3.1. This geometry deformation would require excessive internal machining for the seal to be water tight and the concept was abandoned.

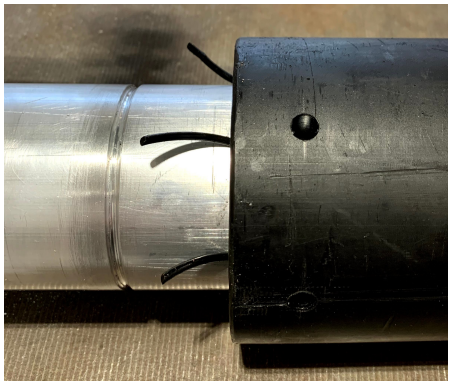

Figure 4.7: Example of O-ring failure do to extrusion during prototyping

External Flange

The external flange connection, with a steel flange and PE adapter is the industry standard HDPE pipe connection method. The adapter is welded on each end of the pipe and a fitted bolted steel flange connection apply evenly distributed pressure on to the adaptors, compressing the gasket in the middle, shown in figure 4.8.

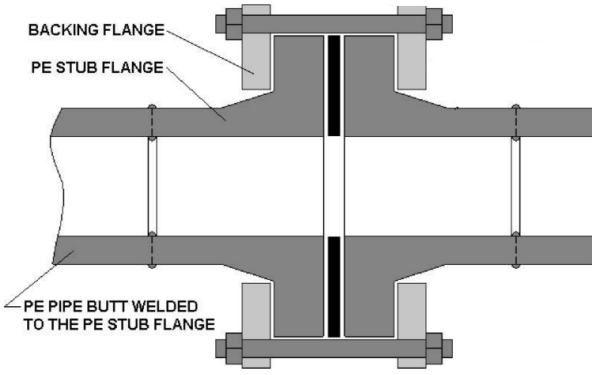

Figure 4.8: A schematic of the external flange connection

This works well for pipelines, as no part of the connection influences the flow inside. For the hull design however, the need for minimal drag is on the outside of the pipe, to achieve an efficient propulsion for the vessel.

An outside flange connection would cut down on cost and build complexity, as they are stock parts and can be ordered directly from a manufacturer. Still, it was decided that the added cost in drag was not worth the benefits in construction.

Internal Flange

The internal flange came as an idea where the intention was to overcome the drawback of the external flange. Slots for bolt connections are cut out of a pipe section with high wall thickness. This results in an effective flange that is flush with the outer diameter, reducing drag. With this design, the bending momentum related to the external flange-adaptor-design will be reduced.

The initial concept of an internal flange connection was developed during a conversation with a company specialised in machining PE pipes, AstorPlast. The initial concept is shown in figure 4.9.

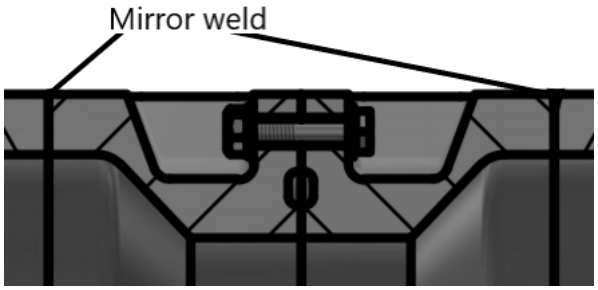

Figure 4.9: A schematic of the initial internal flange concept from AstorPlast

The pipe sections with thicker walls would be machined and then welded onto the main pipes.

Blind flanges were introduced in the connections to introduce redundancy into the hull design. These blind flanges would go between every module and prevent water from a possible leakage to spread. The blind flange needed to be stiff and have a good surface finish as it would compress the O-ring seal.

The internal flange was a more expensive solution than the external flange, but the added hydrodynamic benefits were deemed worth it and the design was carried forward. The full machine drawings of the pipe connections sent to manufacturing are found in appendix A.

4.1.8 O-ring selection

The O-ring is defined by its torus diameter, d_1, and cross sectional diameter, d_2, as explained in 3.3. d_1 was set to $450mm$, as this was the closest available standard length related to the face seal. A bigger cross sectional diameter has higher dimensional tolerances and is also compressed at higher rate. These two factors combined give bigger tolerances in the total connection design as well.

The highest d_2 available from the NTNU O-ring supplier, *Gummi- & maskinteknikk AS*, was $6.5mm$. The O-ring was produced in accordance to **DIN3771-1** and had a dimensional tolerance of $d_2 = 6.5 \pm 0.15$mm.

The O-ring housing was designed according to *Fluid power systems – O-rings – Part 2: Housing dimensions for general applications* [28] resulting in a housing width of 8.4mm and housing height of 5.2mm. This compresses the O-ring 25% of original diameter, 1.3mm.

The O-ring material chosen was FPM. It had a temperature range that met the requirements, good wear resistance and the shortest delivery time. The delivery time was the deciding factor as the goal was to have a working prototype by the end of the project and the estimated delivery dates of the O-rings fell very close to project deadline.

4.1.9 Modelling

The whole hull assembly was modeled in Solidworks, but only the internal flange connection was analysed using FEA, also in Solidworks. The purpose of the analysis was to determine the SDR and number of bolt connections in the joint to ensure that it stayed water tight during bending. The failure criteria was the deflection of the O-ring housing, which was set to half that of the manufacturing tolerance of the O-ring.

Set Up and Constraints

Multiple simplifications were made to the model before analysis. Only the pipe connection was simulated and the rest of the vessel was represented as an external force. As both the pipe and pipe connection is symmetrical the model was simplified to half a pipe fixed through bolt holes to a virtual wall.

The PE100 material was modeled as a linear elastic isotropic material. The material properties used is shown in table 4.3.

Elastic modulus	$1100MPa$
Poisson's ratio	0.4
Yield strength	$23MPa$
Mass density	$959kg/m^3$

Table 4.3: Material properties of PE100.

The pipe part was cut in half and a symmetry constraint was placed upon it. A virtual wall constrain was then placed on the side wall that houses the O-ring stopping any deformations that would intersect the wall. A cylindrical constraint fixing any radial deformation was then placed on the bolt holes. The final constraint is placed on the face around the bolt hole where a washer would be constraining deformation in the normal direction. These two constraints are equivalent to a bolt connection with infinite stiffness, but it should be a reasonable approximation as steel has a much higher stiffness compared to PE 100.

The load placed upon the part was a bending moment of $3kNm$, equivalent to the maximum carry capacity with a moment arm of half the vessel, 1.5m.

Mesh

The mesh type used is what Solidworks calls solid mesh. This refers to a tetrahedral 3D solid element mesh.

A convergence test was done using the $3kNm$ bending moment load. The failure criteria was defined as a set deformation of a node near the O-ring housing. Table 4.4 shows the deflection at that node. The results show a slight increase with mesh size for the first tree mesh sizes, but that trend seems to stop for the final step. This indicates that the convergence of deflection has occurred around the mesh size of $7mm$. Running the simulation with a mesh size of $2mm$ was computationally expensive, as this took well over an hour. For practicality, a mesh size of 7mm was chosen for the detailed analysis.

Table 4.4: FEA of internal flange: mesh convergence test.

Global mesh size $[mm]$	25	12	7	2
Deflection x 10^1 $[mm]$	2.32	2.51	2.62	2.60

4.1.10 Results

The three variables that were changed in this analysis were: number of bolt connections, wall thickness and washer size. There was a stress concentration around the bolt when the washer had a diameter of 12mm as shown in figure 4.10a. This was resolved using a larger washer that distributed the load from the bolt over a wider area 4.10b.

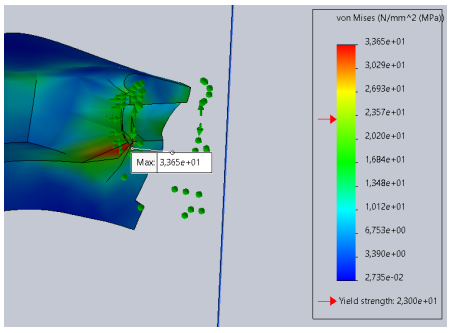

(a) Stress concentration above yield strength around washer.

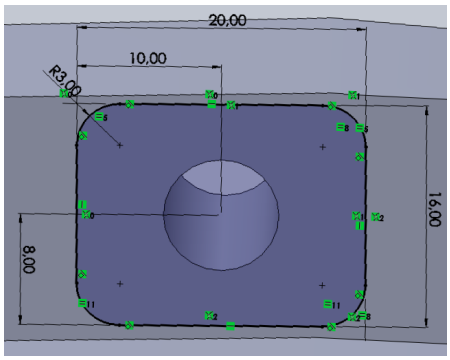

(b) The new washer design.

The results presented in table 4.5 are related to the specially fitted washer. The wall thickness of $29.7mm$ correspond to SDR17 and $45.4mm$ to SDR11. The highest allowable deflection was set to $2.5x10^1mm$, as this equals half the geometric tolerance of an O-ring of $6.5mm$ cross section, this according to **ISO3302-1**.

The 16 bolt design of SDR17 and the 14 and 16 bolt design of SDR11 gave acceptable deflection.

The SDR17 with 16 bolts was chosen because of the weight benefit.

Wall thickness [mm]	**Number of bolts**	**Deflection x 10^1 [mm]**
29.7	12	3.5
29.7	14	2.7
29.7	16	2.3
45.4	12	2.8
45.4	14	2.2
45.4	16	1.9

Table 4.5: The result of the simulations.

4.2 Development of Rudder

4.2.1 Foundation

During the authors project thesis [8] a first prototype of a rudder was designed and constructed in GFRP. The main purpose of this prototype was a feasibility study of manufacturing techniques as well as to serve as the rudder of the first prototype CAT. This rudder was not intended for use outside a few tests, as it was constructed using mild steel for the rudder stock, and this part had limited corrosion resistance.

The aim of this new rudder was to serve as the rudder for the ORCA prototype and it should be designed to follow the vessels hierarchy of design goals, section 1.1. The span, cord, and profile of the new rudder were determined during the project thesis [8] as shown in table 4.6.

Rudder Specifications	
Profile	NACA 0015
Cord length	330 mm
Span length	500 mm
Design rudder load	238 N
Design torque	25 Nm
Safety Factor	2

Table 4.6: Rudder specifications.

4.2.2 Analysis of Rudder Failure Modes

The first step in the rudder design process was an analysis of what failure modes to take into account. This included establishing common failure modes for different types of rudders and what the critical scenarios could be. Through a study of web articles in sailing magazines, [30], and literature [31], [32], a rudder failure mode overview was established, see table 4.7. This overview is limited to reflect modes that are typical for composite rudders, using conventional metal rudder stocks.

1	Rudder stock failure
2	Spoke failure
3	Delamination
4	Bearing failure

Table 4.7: Failure modes of rudders in order of estimated frequency.

Stock failure seemed to be the most common failure mode according to literature. This part transmits torque from the motor and hydrodynamic forces from the water to the bearings.

In conventional ships the stock is made of corrosion resistant steel or aluminium. The two main causes of failure sited is crevice corrosion and fatigue due to cyclic loading. DNV GL [33] found that crevice corrosion is particularly common.

The second most common failure mode is spoke failure. The spokes transmit the torque from the stock to the blade.
The spokes are usually welded onto the rudder stock in different configurations as seen examples of in figure 4.11. These spokes mainly fail due to corrosion or crack propagation through the weld and HAZ. They can also fail due to inadequate torque transmission to the core material of the blade.

Delamination in the composite shell of the blade is the third most common failure mode. The root causes of this failure mode is more diverse, but the typical weak point is the seam where the two halves of the rudder is bonded together. Water ingression and subsequent thaw and freeze cycles during storage is a common way for delamination to occur.

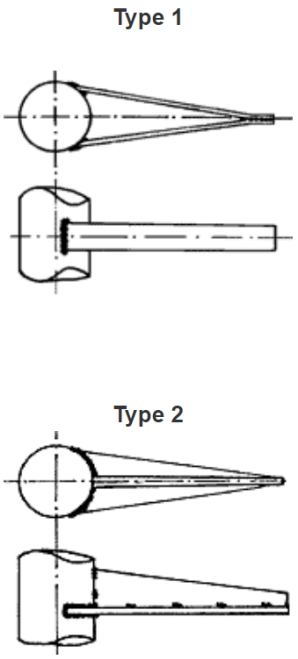

Figure 4.11: A schematic of two common spoke designs [34].

Bearing failure is the fourth most common failure mode cited in literature. This is usually a result of combined corrosion and abrasion over time.

4.2.3 Rudder design

To combat the two most common causes of rudder stock failure, corrosion and fatigue, it was decided to produce the stock in GFRP.

Initial calculations showed that a $20mm$ stock diameter would be sufficient. However, the standard polymer bearings that was decided on, had a minimum inside diameter of $35mm$. For simplicity of design, stock diameter was changed to outer diameter $35mm$ to fit the bearing with minimal machining.

The spokes of the rudder stock were also decided to be made of GFRP. These were to be fitted to the stock using GFRP as well. The spokes consist of two parts; the flat sheet running the length of the rudder ensures transfer of torque from the rudder stock, and the profile shaped fins provide bending stiffness.

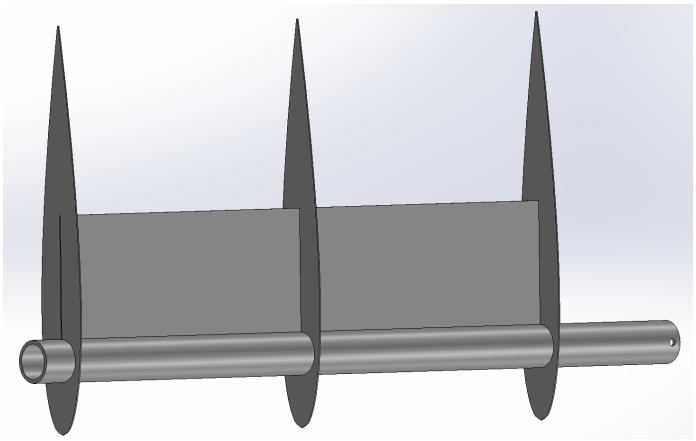

Figure 4.12: SolidWorks model of rudder stock with spoke design.

Glued around the spokes are four foam core sections filling the cavities. Enclosing the hole design is the GFRP shell, which is molded around the core in one process, eliminating the typical lengthwise seam.

4.2.4 Modelling of Rudder Stock

As for the hull, Solidworks was used to create the rudder model. The FEA was done in *Abaqus*, as this software has been designed to also handle laminate elements and thus suitable to simulate composite materials. Two separate analysis were run. One of just the rudder stock, to determine wall thickness and fibre direction, and the second of the complete rudder assembly.

Set Up and Constraints

For the rudder stock analysis the stock was simplified into a small pipe section with diameter 35mm. The geometry was extruded as a shell directly in *Abaqus*. One side of the pipe was constrained in all degrees of freedom. The other side experienced the critical bending and torsion moment with the SF for the rudder. This resulted in a bending moment of $M_b = 65.3Nm$ and a torsional moment of $M_t = 50Nm$. This was to simulated the stresses experienced in the middle of the rudder stock at maximum bending moment, without the added stiffens of the spoke-shell-construction.

The actual fibres, *HiPerTex W2020*, and epoxy, *EPIKOTE MGS RIMR135*, that were to be used in the filament winding process, did not have any combined ply material property values available. However, Silenka E-glass 1200 and epoxy MY750, as described in a filament winding process in Echtermeyer *et al.* [35], are a similar type fibre and epoxy. Thus the combined properties given for this ply was assumed to be a good approximation.

Static ply properties for an unidirectional orthotropic glass fibre-epoxy lamina

were defined according to Figure 4.13.

E1	E2	Nu12	G12	G13	G23
45600	16200	0.278	5830	3770	3460

(a)

Ten Stress Fiber Dir	Com Stress Fiber Dir	Ten Stress Transv Dir	Com Stress Transv Dir	Shear Strength
1140	-570	35	-114	72

(b)

Figure 4.13: (a) Elastic and (b) failure properties of the orthotropic GFRP lamina, as defined in Abaqus. The unit is MPa for all except the unitless in-plane Poisson's ratio Nu12.

The rudder stock was to be produced on a filament winder. This limited the possible lay-up patterns to hoop and helical. To simulate hoop lay-up a layer of unidirectional plies perpendicular to the length of the tube were used. To simulate helical lay-up, adjacent $[\pm 45^o]$ layers were used to mach the angel of the helical program. The thickness of one winding cycle in the filament machine were estimated to be $1mm$. This means that a single layer in the simulation were to be $0.5mm$, as one layer only incorporated one of the directions of the lay-up.

Mesh

The shell mesh used was quad dominant. This entailed that the geometry was mainly mapped with S4R elements, but S3 could be used by the algorithm.

To find the minimum rudder stock thickness needed to achieve necessary strength, the convergence test was done applying the Tsai-Hill failure criteria. The same boundary conditions and forces as for the final analysis were applied. The results are presented in table 4.8.

Global mesh size, *mm*	8	5	2
TSAIH x 10^1	6.17	5.75	5.76

Table 4.8: FEA of rudder stock: mesh convergence test using Tsai-Hill failure criteria (TSAIH).

The value of failure criteria changes 7% from 8mm mesh size to 5mm mesh size, but in the next step it changes only 0.1%. This indicates that convergence of the Tsai-Hill index before and/or close to a size of $5mm$. An element size of $5mm$ was decided for the simulation.

4.2.5 Results

The rudder stock must have bending and torsional strength. Four different ply stacking sequences were tested. The results are shown in table 4.9. As the SF was incorporated into the loads, a Tsai-Hill index, $I_F^{T-H} \leq 1$ is sufficient. Only the 1mm thick $\pm 45^o$ laminate failed the test.

$[\pm 45^o]$	1.38
$[\pm 45^o, 90^o, 90^o]$	0.765
$[\pm 45^o]_2$	0.617
$[\pm 45^o]_3$	0.382

Table 4.9: Lamina lay-up with resulting Tsai-Hill index.

The results indicate that hoop winding does not increase strength as much as helical winding does for this load criteria. As both winding types consume approximately the same amount of material, it was decided to have a pure helical winding layup.

A $2mm$ thick rudder stock with a $[\pm 45^o]_2$ winding pattern would be adequate. However, since the closest suitable mandrel material, a standard PE-pipe, had a $32mm$ outer diameter, the stock design ended up with a $3mm$ thickness and the $[\pm 45^o]_3$ lay-up.

4.2.6 Modelling of whole Rudder

The analysis of the complete rudder assembly was done to determine the of number spoke profiles to be applied, as well as spoke and shell laminate thickness and orientation.

The foam core was not incorporated into the analysis as the strength contribution was expected to be at a small scale, and at the same time would complicate the modeling process. The resulting strength deviation for the model versus the physical rudder, related to omitting of the core in the modeling, will be in a conservative direction and deemed acceptable.

Set Up and Constraints

The model assembly of the rudder was converted from solid to shell geometry and exported as .STEP files to *Abaqus*. The skin and spoke parts were connected to the rudder stock and each other through tie constraints. A consisted definition of constraints, master to slave surface, is necessary for the connection to function in *Abaqus*. Thus a surface to node region tie with a master to slave hierarchy was defined. The rudder stock or whichever part was closest to the rudder stock, was designated as master surface, and the hierarchy became; stock, spoke plate, spoke profiles and shell.

The model was set up with rigid (no rotation and no displacement) boundary condition on one end of the stock, free rotation and otherwise fixed (no displacement) on the other end. These boundary conditions approximated the bearing fastening at each end of the rudder. The force applied to the model was a static distributed load on one of the shell faces. The total magnitude of the force was $476N$, which equals the dimensional load multiplied with the SF.

The material properties used for the unidirectional orthotropic glass fibre-epoxy lamina were also collected from Echtermeyer *et al.* [35]. For this case the chosen properties, shown in figure 4.14, is for a VARTM ply with the same epoxy system, EPIKOTE MGS RIMR135, as the actual build. The fiber used in the relevant ply in Echtermeyer *et al.* [35] are of a comparable type as the actual build, both common E-glass, so the *Abaqus* simulation should be relatively accurate for this VARTM construction.

E1	E2	Nu12	G12	G13	G23
44600	1700	0.262	3490	3770	3460

(a)

Ten Stress Fiber Dir	Com Stress Fiber Dir	Ten Stress Transv Dir	Com Stress Transv Dir	Shear Strength
1240	774	43.9	179	55.8

(b)

Figure 4.14: (a) Elastic and (b) failure properties of the orthotropic GFRP lamina, as defined in Abaqus. The unit is MPa for all except the unitless in-plane Poisson's ratio Nu12.

All composite parts of the rudder, except the rudder stock, was made with the VARTM process. These laminates were to use a combination of $[0^o/90^o]$ woven roving and $[\pm 45^o]$ biaxial fabric. The $[0^o/90^o]$ fabric was EC933X1TEX from Easy-composites, and the $[\pm 45^o]$ biaxial fabric was Saertex X-E-302g/m^2. The full data sheets of the materials are given in appendix B.

The thickness of the two fabrics were measured to be 0.2 mm thick for the $[0^o/90^o]$ sheets and the $[\pm 45^o]$ sheet was found to be 0.25mm thick. In the model, pairs of UD plies, half the measured thickness, were rotated to the matching angel to simulate the two fabrics. This is standard practice for such calculations, as it can be expected to give reasonable results, ref. Lasn *et al.* [36].

The data used for the rudder stock in this simulation was the same as in the simulation discussed in section 4.2.4.

Mesh

The mesh type used during this analysis was the same as used during the rudder stock analysis, quad dominant.

The limiting factor of the rudder design, apart from the stock design and stock bearings - as discussed in section 4.2.2, was the strength of the spoke fins. These also showed to represent the largest stress concentrations during simulations. To keep processing times down then, the convergence test was done with only changing the element size on the spoke fins. The element size used for the other parts can be found in table 4.10. Again, Tsai-hill was used as the criteria during the convergence test, table 4.11.

Rudder part	**Element size**
Rudder stock	5mm
Spoke plate	50mm
Rudder shell	25 mm

Table 4.10: Element size used for rudder FEA.

Global mesh size, *mm*	10	5	3	1.5
TSAIH x 10^1	3.97	5.20	5.81	5.96

Table 4.11: FEA of full rudder: mesh convergence test using Tsai-Hill failure criteria (TSAIH).

The results show an increasing trend with smaller element size. This trend is decreasing however, indicating that convergence of the Tsai-hill index is happening at the smaller element sizes. The computational cost of using an element size of 1.5mm was deemed too great, and an element size of 3mm was used for the spoke fins.

4.2.7 Results

The maximum Tsai-hill index measured in the simulation was 0.64, which is bellow 1, and satisfies the strength criteria of $I_F^{T-H} \leq 1$. This occurs in the connection between the rudder stock and the spoke fin nearest to the bearing that is bound in both translation and rotation. The resulting Tsai-hill index, that can be seen in figure 4.15, is around 0.3 for the shell and 0.45 for the other spoke fins.

The simulation does not reflect the rudder shells true bending stiffness since the foam core is omitted from the equation. In the simulation the 0.45mm thick shell deforms 11 mm in a cave in between the spoke fins. These results are unrealistic and conservative as the shell would be supported by the foam.

The lay-up used for the simulation is as shown in table 4.12.

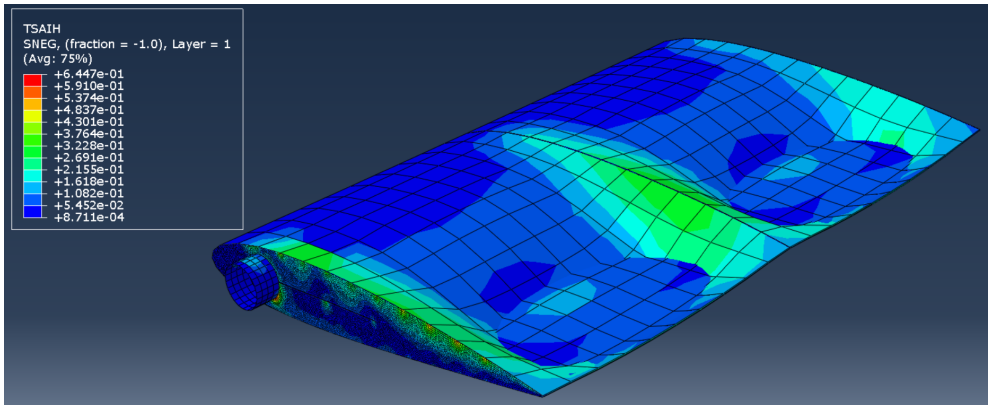

Figure 4.15: Tsai-Hill index of rudder subjected to a hydrodynamic force of 476N.

Rudder part	**Lay-up**
Spoke fin	$[0^o/90^o/\pm 45^o]_{Sym}$
Spoke plates	$[0^o/90^o/\pm 45^o]_{Sym}$
Rudder shell	$[0^o/90^o/\pm 45^o]$

Table 4.12: Lay-up used for the rudder.

4.3 Skeg development

4.3.1 Foundation

A full skeg design was decided upon during the author's project thesis [8]. Durability of the rudder fastening methods had first priority when deciding on the design.

A skeg runs the full span length of the rudder and must have a fastening at the bottom of the rudder stock, as shown in figure 4.16.

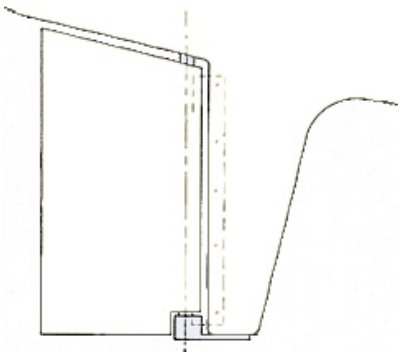

Figure 4.16: Schematic of full skeg from [37].

The skeg's purpose is to protect the rudder from incoming debris and take up

bending moment from the hydrodynamic forces and transfer this to the hull.

In a generic skeg design it is fastened to, or is a part of, the hull and is connected to the rudder only with the lower stock bearing. As the ORCA project has a hull made of a highly ductile material, PE 100, it will be necessary for the skeg to take up the direct bending moment both at the top and bottom bearings that connect to the rudder stock. Thus the bending moment from the rudder can be redistributed through the skeg to the hull on a large surface and through a high number of fasteners. In this way the forces on one single fastener and also the rudder stock seal, will be well under the hull material limits.

As the skeg is placed before the rudder it is the skegs frontal area that meets the fluid stream first and should therefore be designed in such a way as to minimize drag and increase vessel stability and maneuverability.

4.3.2 Skeg Design

As a full skeg in many ways works as a secondary keel,[38], it was designed using design principles for keels. The most commonly used keel profile is a NACA profile. The NACA profile chosen was the NACA0015 profile. The hydrodynamic benefits of this profile was explored in the project thesis [8].

The skeg consists of a lofted geometry between two NACA0015 sections with varying cord lengths, as shown in figure 4.17. The lower profile was swept back relative to the top NACA profile, as this profile only needed to be wide enough to house the rudder bearing. The NACA profiles were cut of after intersecting with the rudder stock and space was made for the leading edge of the rudder to rotate freely. The skeg specifications can be found in table 4.13.
As the skeg was to be mounted onto the hull pipe, a flange with a curvature matching the outside diameter of the pipe was made. To ensure a watertight seal, a bolted connections to metal threaded inserts was designed. The bolt connection used eight M8 bolts of corrosion resistant steel, matching that of the threaded inserts.

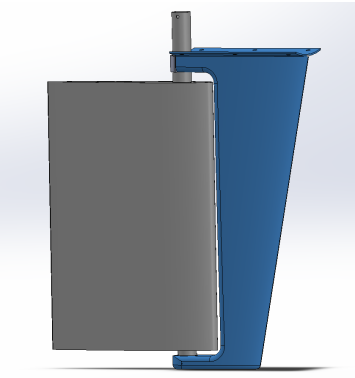

Figure 4.17: The Solidworks model of the skeg.

Skeg Specifications	
Profile	NACA0015
Upper cord length	480 mm
Lower cord length	370 mm
Draft	585 mm
Sweep angle	10.5^o
Design skeg load	340 N
Safety Factor	2

Table 4.13: Specifications of the skeg.

The skeg was designed in such a way that both it and the rudder could be assembled and disassembled easily. The rudder can be slotted into the bearing in the bottom of the skeg. The rudder is then secured by fastening the bearing at the top of the rudder to its housing in the skeg.

The initial design contained a sandwich construction with a GFRP shell and PVC closed cell foam core. The core was to be machined on the "Verkstedteknisk" lab CNC-machine, but this was taken out of service for relocation during the project. As the production had to be moved to the "Materialteknisk" lab, the production of the foam was delayed. This necessitated a redesign of the manufacturing process of the shell in order to meet the project deadline. The new production method used for the skeg shell was prepreg CFRP. The flange was still made with GFRP using the VARTM process as originally planned.

The critical load of the skeg was set as the combined hydrodynamic force from the rudder and skeg. As the forces on the rudder is transferred to the skeg through the bearings. The design load scenario was the same as for the rudder, section 1.4. The resulting load is given in table 4.13.

4.3.3 Modelling

As the critical load section of the skeg was found to be the flange connection to the hull, the design could be simplified with regard to the FEA Abaqus analyses. The flange experience the largest bending moment, as the skeg act as a cantilevered beam with a distribution of pressure.

Set up and constraints

A simplified model of the flange and upper skeg was made in Solidworks, as shown in figure 4.18. The flange curvature was flattened and the NACA profile was simplified and divided into distinct sections. The foam core was not considered for the same reasons as layed out in section 4.2.6. The model was then transformed into a shell geometry and exported as a .STEP file to Abaqus.

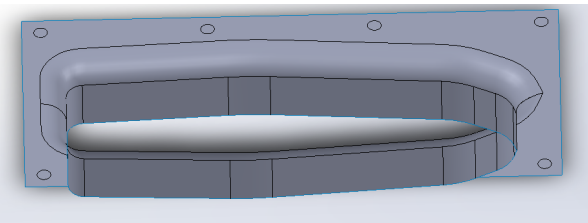

Figure 4.18: Simplified shell model of skeg flange in Solidworks.

A boundary condition constraining all degrees of freedom was placed upon the surfaces where bolt holes would be. The edge of the skeg profile was constrained with a coupling constraint to the center of pressure. The center of pressure was estimated to be located 250mm down from the base of the flange and 130mm behind the front edge of the skeg profile. The force applied in the calculations was found by multiplying the design load with the SF. This force, 680N, was applied to the center of pressure.

The material properties used for the flange was the same as for the VARTM parts of the rudder in section 4.2.6. The same production methods and resin was used for the flange as the rudder parts. The prepreg carbon fiber material properties used were *XC110 210g Twill 3k* and *XC110 416g Twill 6k*. The 210g twill is a surface ply and the 416g twill is a backing ply. The material properties stem from Mark [39], who conducted material tests on these materials, presented in figures 4.19 and 4.20.

E1	E2	E3	Nu12	Nu13	Nu23	G12	G13	G23
58000	58000	7500	0.05	0.3	0.3	3300	3300	3500

(a)

Ten Stress Fiber Dir	Com Stress Fiber Dir	Ten Stress Transv Dir	Com Stress Transv Dir	Shear Strength
521	483	521	483	64.7

(b)

Figure 4.19: (a) Elastic and (b) failure properties of the backing CFRP laminate using engineering constants, as defined in Abaqus. The unit is MPa for all except the unitless Poisson's ratios Nu.

Plies of alternating $[0^o/90^o]$ direction was used to simulate the woven glass fabric in the skeg flange as explained in section 4.2.6. The glass fibers used, stocked at the NTNU Composite lab, showed to be of an unknown brand and assumed to have the properties of generic E-glass. The prepreg material was modeled using engineering constants, not lamina theory, and was therefore simulated using one ply per cloth. The thickness of the different cloths were measured and are presented in table 4.14.

E1	E2	E3	Nu12	Nu13	Nu23	G12	G13	G23
53000	53000	7500	0.05	0.3	0.3	3300	3500	3500

(a)

Ten Stress Fiber Dir	Com Stress Fiber Dir	Ten Stress Transv Dir	Com Stress Transv Dir	Shear Strength
521	483	521	483	64.7

(b)

Figure 4.20: (a) Elastic and (b) failure properties of the surface CFRP laminate using engineering constants, as defined in Abaqus. The unit is MPa for all except the unitless Poisson's ratios Nu.

Fabric	Thickness [mm]
XC110 210g Twill 3k	0.25
XC110 416g Twill 6k	0.45
Generic E-glass [0/90]	1
Generic E-glass [±45]	0.5

Table 4.14: Thickness of each fabric used for the skeg.

Mesh

The mesh used was quad dominant like the other Abaqus simulations. As flange failure is the critical part in the skeg design, the Tsai-hill index was applied for a convergence test. The simulations showed that stress concentration will form at the bolt hole edges, so local seeds with a smaller mesh size was placed on these, see figure 4.21. The seed mesh size represented the variable during the convergence test. The rest of the flange were given a mesh size of 10mm.

The result of the convergence test, table 4.15, shows no declining or increasing trend in stress. The scatter of the first two results are quite large, while the two smallest mesh sizes indicate convergence. If we plot the results in a 2D coordinate

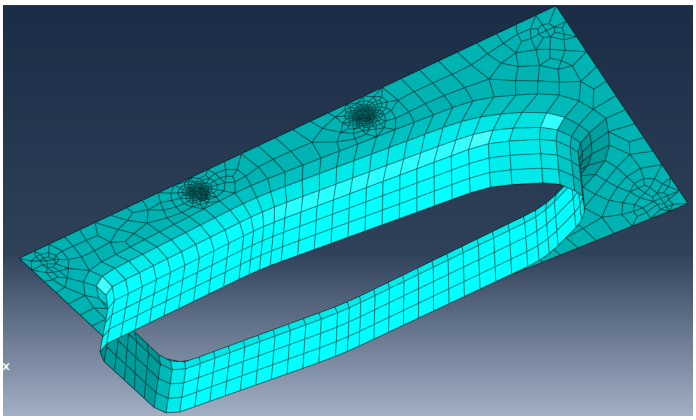

Figure 4.21: Mesh of skeg geometry in Abaqus.

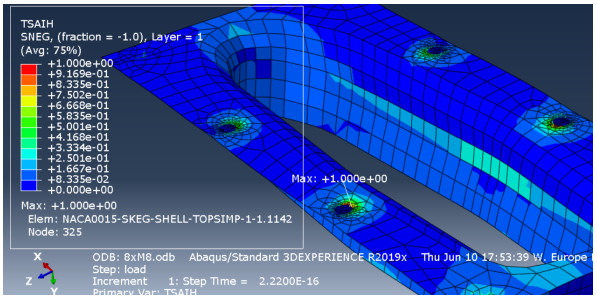

Figure 4.22: Results from FEA of the Skeg.

system, this would be presented as an oscillating divergence. This convergence happen between a mesh size of 1mm to 0.5mm, Where a mesh size smaller then 0.5mm will give acceptable results. Thus the 0.5 seed was used for the simulation.

Seed mesh size, mm	2	1	0.5	0.3
TSAIH x 10^1	9.24	8.49	10.0	9.98

Table 4.15: Results from convergence test of skeg mesh.

Results

Different lay-up combinations and bolt hole placements where simulated. The design satisfying the strength criteria for the skeg had the lay-up presented in table 4.16.

Skeg part	**Lay-up**
Flange	$[0^o/90^o/\pm 45^o/0^o/90^o]$ E-galss
Body	$[0^o/90^o]$ Carbon top, $[0^o/90^o]$ Carbon backing

Table 4.16: Lay-up of skeg.

Three plies of E-glass was used in the flange. The prepreg carbon layup used for the body of the skeg consisted of one backing ply and one surface ply. 8 bolts were found to be sufficient to fasten the skeg to the hull. The maximum Tsai-Hill index in the simulation was $I_F^{T-H} = 1$, as shown in figure 4.22. This is just within the acceptance criteria.

The maximum reaction force in the bolts were 375N. This is only 7% of the proven pull out strength of the inserts, see section 4.1.4, and the construction is acceptable for the simulated load case.

4.4 Development of Rudder Actuation System

4.4.1 Design limitations

During the actuation system design startup phase several key design limitations and specifications were defined. The first one being that the actuation system should integrate with the internal storage tray system of the hull and have its own modular pipe compartment. This limited the actuation systems size to a tray with the size of 245 X 380mm.

The actuation system specifications in table 4.17 were defined. The positional accuracy was defined to mach that of the vessels wind sensor. The minimum angular velocity was derived by setting four seconds as the longest time the rudder could use from one extreme range of motion to the other. Both range of motion and design torque was defined in the project theses [8].

Rudder actuation specifications	
Positional accuracy	2^o
Minimum angular velocity	$15^o/s$
Range of motion	60^o
Design torque	25Nm
Safety Factor	2

Table 4.17: Specifications of rudder actuation system.

4.4.2 Actuator

Initially, a servo DC motor was planned to serve as actuator for the rudder. The motor chosen was RMD-X8-Pro, from Gyems, and was chosen based on the work done by S. Gauden in [7]. This motor was to drive the rudder directly as shown in figure 4.23. However, this design was abandoned as two servo motors broke and delivery time for new ones, sent from the supplier in China, was too long to meet the project deadline.

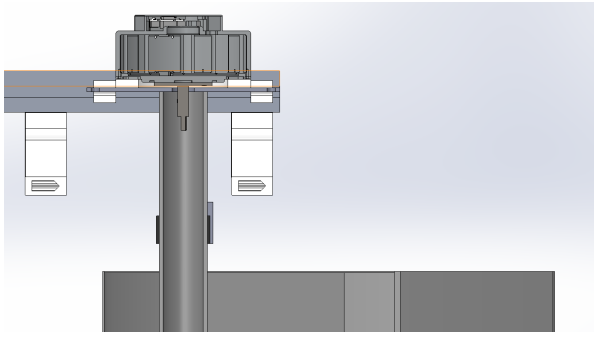

Figure 4.23: Solidworks model of direct transmission from Servo motor to rudder.

The replacement was a Linak LA33 linear actuator. This is a medium sized actuator designed for use on yachts, thus also corrosive environments, making it well suitable for this project. The actuator has a integrated brake, ensuring no power usage when the actuator is turned of. The main specifications of the LA33 are presented in table 4.18, and the full product configuration can be found in the appendix B.

Load	2250 N
Speed	$21mm/s$
Stroke length	100 mm
Stroke Tolerance	$\pm 2mm$

Table 4.18: LA33 specifications.

The linear actuator was connected to a lever arm through a swivel joint, this was fixed to the stock and thus rotated the rudder when the linear actuator extends and contracts. Se figure 4.24. The torque, positional accuracy, range of motion, and angular velocity are all determined by the length of the lever arm and the specifications of the actuator.

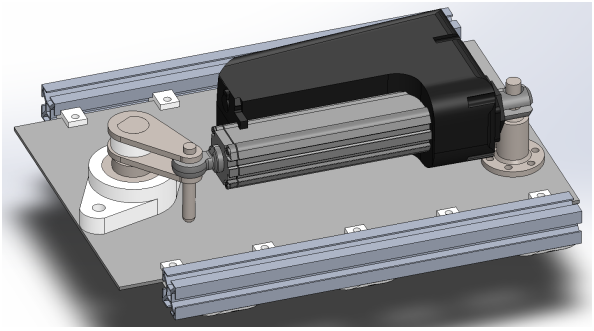

Figure 4.24: Solidworks model of linear actuator system.

The minimum lever arm length was found by calculating the relationship between linear actuation tolerance and angular tolerance for the rudder. The stroke length of the actuator when connected to the lever arm can be thought of as the arc length of a circle with the radius of the lever arm. Using an arc length formula, the minimum lever arm length is:

$$r = \frac{ST \cdot 360}{2\pi\theta} = 57.3mm \tag{4.1}$$

ST is stroke tolerance and θ is minimum positional accuracy for the rudder. A lever arm of 58mm was deemed maximum due to the space constraint of the tray width. In table 4.19 the achieved properties of the actuation system are given.

Rudder actuation properties	
Positional accuracy	2^o
Angular velocity	$20.6^o/s$
Range of motion	60^o
Torque	130.5Nm

Table 4.19: Rudder actuation properties.

4.4.3 Actuator fastener

The linear actuator is fastened thought its back fixture with a cylindrical fastener. This fastener was made using AISI 316 ally steel to be corrosion resistant. The critical load used while calculating fastener strength was the maximum rudder torque transferred through the lever arm. The rudder stock torque is $25Nm$, see 4.17, with a SF of 2, the calculation torque is $50Nm$. The torque produced by the actuator far exceeded the torque load from the rudder, and the rudder is well within the design criteria.

The load calculations were done with FEA in solidworks. The material properties used were that of AISI 316. Linear elastic behavior was assumed. Von Mises was used as a failure criteria.
The joint could even hold the full torque of the actuator, $130Nm$, as this gave a maximum of 99.6 MPa von Mises stress, as shown in figure 4.25.

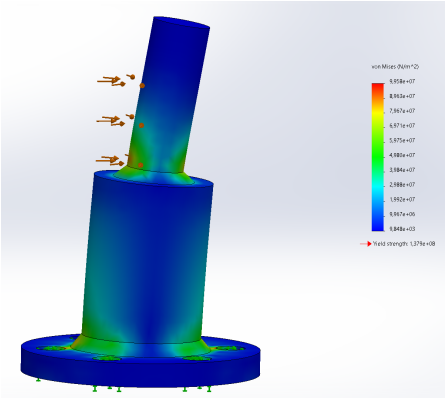

Figure 4.25: Results from FEA in Solidworks

4.4.4 Lever Arm

The lever arm was designed to connect with the linear actuator trough a pin swivel joint. To reduce the bending stresses of the pin, two moment arms were placed on either side of piston rod eye, as can be seen in figure 4.24. The lever arms were to be slid down the shaft in slots, securing them in position. A spacer was 3D printed to fit between the lever arms, and ensure the spacing between them matched that of the rod eye. All the parts in this assembly was also made of AISI 316L steel as to avoid galvanic corrosion, and for the possibility of welding during assembly.

4.4.5 Rudder Bearings

There were three bearings holding the rudder stock. One was fastened to the rudder actuation tray inside the hull. This bearing was a ball bearing in AISI 316 steel.

The two other bearings were polymer bushings fastened to the skeg. One at the top of the skeg and one at the bottom. The bushings chosen were Iglide plastic bushings from Igus. These bushings have great abrasion resistance and does not corrode as metal bearings do. They are used in the fish processing industry on roller conveyors and should prove to be durable.

4.4.6 Shaft Seal

A shaft seal was intended as the waterproofing mechanism around the rudder stock. Traditional rudder seals used for sailing vessels are stuffing boxes, which uses locking nuts filled with sealing rings. These stuffing boxes has a tendency to drip, and can not be made to be leakage free. A shaft seal on the other hand can be made drip free. The saft seal works by clamping a stainless steel rotor onto the rudder stock. This steel rotor is what interfaces with O-rings in an outer steel housing in a dynamic seal. Figure 4.26 shows schematic of a shaft seal used on a rudder. A shaft seal was to be bought as it is a complex assembly with high tolerances, and would require too much manufacturing time. The purchasing of a shaft seal was not done due to time constraints.

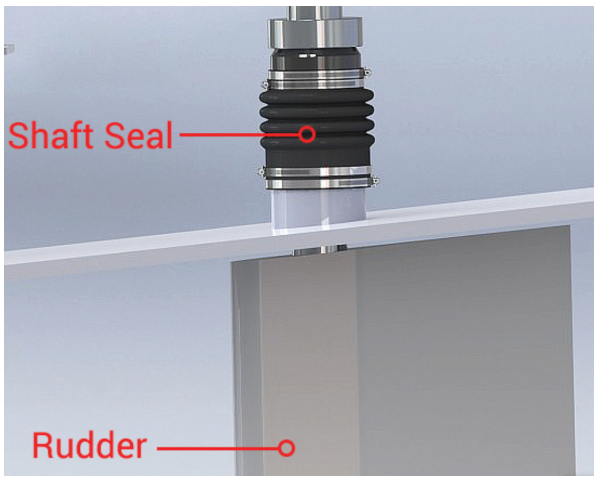

Figure 4.26: Schematic of rudder seal from a manufacturer, [40].

Chapter 5

Manufacturing

This chapter describes the manufacturing process of the hull and rudder prototypes. The steps taken in manufacturing the hull, the rudder, the skeg, and the rudder actuation system is described.

The chapter is organised according to type of process as many of the same production methods were used for multiple parts. A full overview of every polymer and composite manufacturing method used in relation to the parts manufactured can be found in figure 5.1. The general manufacturing procedure is described for each process and notable exceptions and specifics of each part will be given.

		VARTM	Mouldless VARTM	Filament winding	Hand layup	Adhesive joining	3D printing
Hull	Storage tray	x					
	Storage glider						x
	Profile support						x
	Blind flange	x					
Rudder	Rudder stock			x		x	
	Spokes	x				x	
	Shell		x				
Skeg	Flange	x				x	
	Shell				x	x	

Figure 5.1: A matrix of parts manufactured and method used.

The pipe sections for the hull was machined and mirror welded by AstorPlast, so this part of the manufacturing process will not be covered in this thesis. The parts of the hull that was manufactured by the author during the master project, was the internal storage trays and the blind flanges and these are described in the following sections.

As all composite parts made during this project needed post processing, this is presented. An overview of the manufacturing of the non-composite parts is given. The assembly process for the hull and the rudder is described and at the end of the chapter an estimation of cost is presented.

5.1 VARTM

VARTM was used to manufacture the storage tray sheet and the blind flanges for the hull and spokes for the rudder and the skeg flange. The particular VARTM method used was a VARTM with flow mesh, described in section 2.2.1. The VARTM process was chosen as it has several benefits over hand lay-up and resin transfer molding. It produces higher quality, repeatable and more consistent parts compared to the hand lay-up, and is a more flexible and salable alternative to resin transfer molding [12].

All the parts made by the VARTM method had simple geometries that did not need special moulds to be made. All these parts, except the skeg flange, were planar and could therefore be made using a flat metal sheet as a mold. The mould used for the flange was the outside of the pipe hull, to ensure an accurate curvature. This reduced manufacturing time and cost significantly. Another benefit was the simplification of the infusion process as no flow simulations were needed to predict the flow pattern through the part.

5.1.1 Materials Selection

All parts made with the VARTM process used the same DNVGL approved resin system, EPICOTE™Resin MGS™RIMR135 together with EPICURE™Curing Agent MGS™RIMH137 and/or RIMH134. The resin system is designed for infusion processes and is sutable for wind turbine blades, ship building, etc. A feature of this resin system is its long gelation time, which allows for the relaxation of the part during the post filling stage. A full data sheet for the resin system can be found online [41].

An epoxy resin system was chosen over a polyester system for several reasons. Epoxy systems are less dangerous as they do not emit poisonous gasses. The epoxy systems also offer superior strength and has a lower water absorption rate compared to polyester systems [42].

The fibers used in the VARTM process varied from part to part. An overview of glass fiber colths and weaves used is given table 5.1. The two fiber cloths de-

scribed as generic E-glass were rest cloths from earlier projects where the material documentation had been lost. The decision to use these material was made as the parts that used them needed to be thick, and stacking multiple thinner cloths would have been very expensive and time consuming. The estimated material properties of the generic E-glass cloths is discussed in section 4.3.3.

Material	**Weave orientation**	**Thickness**	**Usage**
Easycomposites 200g 2x2 Twill Woven	[0/90]	0.2 mm	Rudder spoke
Saertex X-E-302g/m^2	[±45]	0.3 mm	Rudder spoke
Generic E-glass 0/90	[0/90]	1 mm	Storage tray, blind flange, skeg flange
Generic E-glass ±45	[±45]	0.5 mm	Storage tray, blind flange, skeg flange

Table 5.1: Fibers used in VARTM process.

5.1.2 Process parameters

An overview of the different process parameters used is given in table 5.2. The other steps used during the VARTM was constant for all transfusions.

The size of the laminate sheets were chosen so there would always be a minimum of 5cm clearance between the final part and the edge of the laminate. This was to ensure that the part avoided areas of the laminate with dry spots or fabric folds/ miss alignment.

The amount of resin needed was calculated using the volume of the fiber cloth and the fiber volume ration. The formula,

$$M_r = \rho_r \frac{v_r}{v_f} V_{tot}, \tag{5.1}$$

used a conservative fiber fraction(v_f) of 0.4, and epoxy density (ρ_r) of 1.3$\frac{g}{cm^3}$. This equation would overestimate the resin in the part, and this compensated for the resin loss in the consumables. This method worked great for bigger molds, but tended to under compensate for the loss do to consumables. For the two smallest VARTMs, the rudder spokes and skeg flange, some additional resin was added on top of what was calculated.

The first big VARTM chronologically was the first blind flange batch. This used two inlets and two outlets. Using two inlets proved to be impractical as the resin

Part	Storage trays	Blind flange 1	Blind flange 2	Rudder spokes	Flange
Size $[mm]$	600 x 1160	600 x 1200	600 x 1200	360 x 560	240 x 350
Lay-up thickness $[mm]$	3	3	3	0.9	2.5
Resin mass $[kg]$	4.7	5	5.1	0.5	0.6
$\#inlets$	1	2	1	1	1
$\#outlets$	2	2	3	1	1

Table 5.2: VARTM process parameters

was sucked into the mold quicker. This made it hard to close the inlet before the buckets emptied of resin, resulting in a small amount of air getting into the part. The leaked air did not seem to degrade the final quality of the part much. It is assumed that the extra air was trapped in the flow mesh, while the fibers underneath remained saturated with resin.

One inlet combined with a resin flow spiral was used for the rest of the VARTM parts, as pictured in figure 5.2. This resulted in a slight increase in wasted resin as the resin traped in the flow spiral was thrown away, but the improved process control was deemed worth it.

The surface finish from the VARTM was good on the mould side. The peal ply side was rough, with surface texture like that of 80 grit sandpaper. This was sufficient for all parts except the blind flanges. The flanges needed a smooth surface to seal properly.

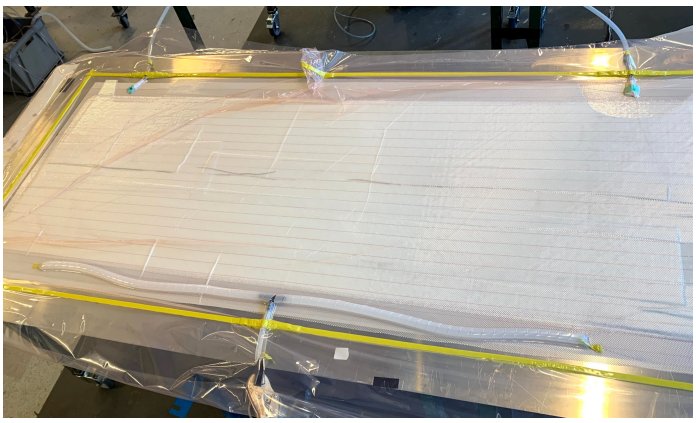

Figure 5.2: Picture during vacuum test of VARTM of storage tray.

5.2 Mouldless VARTM

The manufacturing method chosen for the rudder was a mouldless VARTM process. This decision was made despite the drawbacks mentioned in section 2.2.2. The economical and time advantages of not having to make a mould for a prototype was the main reason why the method was chosen. A relatively stiff foam combined with a rigid spoke construction was used to combat the warping during curing the mouldless method is prone to. The diminished surface quality of the mouldless method was not weighed heavily as it was a prototype and surface quality was not expected to have a great effect on the performance.

5.2.1 Material Selection

The resin system used for the Mouldless VARTM was the same as for the regular VARTM, described in section 5.1.1. The fibers used was the Easycomposites 200g 2x2 Twill and Saertex X-E-302g/m^2 from table 5.1.

As a core material *MyCell 80kg* closed cell PVC foam from Maricell was used. This is a core material commonly used in the marine industry as it has a very low water absorption, and a good compressive strength of $1.22MPa$. The material technical data sheet of the foam can be found in the appendix B.

5.2.2 Test infusion

As the author had never done a mouldless VARTM before, a test infusion was done. This test infusion used a solid piece of the *MyCell 80kg* foam cut in a similar shape to the rudder and the same fiber lay-up as in the final rudder.

The process started by wrapping the foam core with the glass fiber sheets. A spray adhesive, *FusionFix GP Spray Adhesive*, was used to bond the cloth to one end of the trailing edge. The cloth was then pulled tight over the foam core and adhered to the same side of the trailing edge using the same adhesive. The same process was done for both the glass fiber cloths.

The fiber clad part was then wrapped in peel ply and flow mesh, before the whole assembly was put into a prepared vacuum bag, figure 5.3. The inlet was placed on the leading edge of the rudder mock up and the outlet was placed approximately 50mm away from the trailing edge, to ensure full infusion of the part before the resin reached the outlet. The inlet had a T-joint at the end and was wrapped in felt to ensure resin flow into the part.

The normal VARTM process was then followed with a pressure test, infusion, and curing under vacuum pressure. The result of the test infusion can be seen in figure 5.4.

Figure 5.3: Test infusion during vacuum bagging.

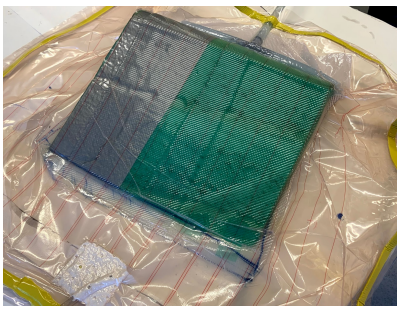

Figure 5.4: Fully cured mouldless VARTM test infusion.

The test infusion was insightful and several practical lessons were learned during the process. The process parameters that could be improved were:

- Oversize the vacuum bag compare to the geometry. Creation of folds allows the bag to better compact around the core.
- Place the inlet a distance away from the part. When the inlet in placed at the part surface the vacuum bag stretches around the inlet and does not properly compact the fibers to the core, resulting in air bobbles between the fibers and the core.
- Have a greater overlap of sheets at the trailing edge of the rudder. This ensures a stronger bond and makes the fiber lay-up much easier.
- Use the spray adhesion liberally, on both the trailing and leading edge. Avoiding folds and creases is much easier when the fabric is secured in several places.

5.2.3 Final Transfusion

The final transfusion was done by wrapping the rudder core in the same way as the test transfusion described in section 5.2.2. Learning from the test transfusion the glass cloth was wrapped around the trailing edge with a minimum of 5cm clearance, pictured in figure 5.5.

The other process improvements from the test infusion were also followed and an overview of the rudder mid infusion can be seen in figure 5.6. The rudder shaft had to be sealed during infusion to be able to pull a vacuum. A double seal was implemented, one inside the vacuum bag and one in the other end of the rudder stock.

The process parameters used is presented in table 5.3. The resin mass was calculated as described in section 5.1.2.

The results from the mouldless VARTM were of high quality. There were no dry spots of air bobbles visible. The shell had been compacted into the core structure and no cavities or bridging could be found. Wrinkles were not found on the surface

Fiber Size $[mm]$	540 x 780
Lay-up thickness $[mm]$	0.45
Resin mass $[kg]$	0.4
# inlets	1
# outlets	1

Table 5.3: Mouldless-VARTM process parameters.

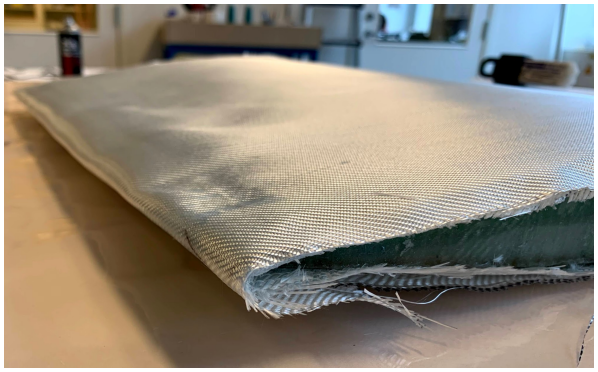

Figure 5.5: A close up of the cloth overlap at the trailing edge of the rudder.

of the part, but there was some fringing outside of the core edge as figure 5.7 shows. This fringing was easily cleaned up in the post processing.

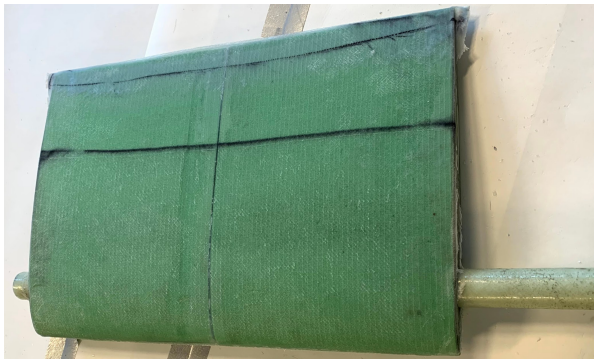

Figure 5.7: Overview of mouldless VARTM mid transfusion.

Figure 5.6: Overview of mouldless VARTM mid transfusion.

5.3 Filament winding

Filament winding was chosen as the manufacturing method of the rudder stock. This was because of the repeatability and quality stability mentioned in section 2.4. The disadvantage to this production method was the high time investment as both the winding program and a mandrel had to be made from scratch. These two processes were very time consuming and a hand lay-up of either prepreg or wet fibers would have been preferable as a prototype manufacturing method.

5.3.1 Material Selection

The epoxy resin system used during filament winding was the *EPIKOTE MGS RIMR135* system, described in section 5.1.1. This resin system works well for filament winding as well as the long gelation time give some extra leeway during the winding process, as this can often take multiple hours.

The fiber used was *HiPerTex W2020* produced by *Binani and 3B*.

5.3.2 Mandrel Construction

First mandrel

The mandrel was originally fabricated in house from a steel rod on a lathe. The mandrel was made according to the specifications in table 5.4, explained with figure 5.8. An attempt was made to make the mandrel slightly conical with one end of the mandrel length having a outer diameter of 31mm and the other having a diameter of 32mm as specified. This is a standard procedure and makes the demoulding process much easier. A smooth surface finish is also important for demoulding as it reduces mechanical locking.

Mandrel specifications	[mm]
Outer diameter	32
Minimum end length, L_e	200
Filet length, L_f	20
Mandrel length, L_m	728

Table 5.4: Mandrel specifications.

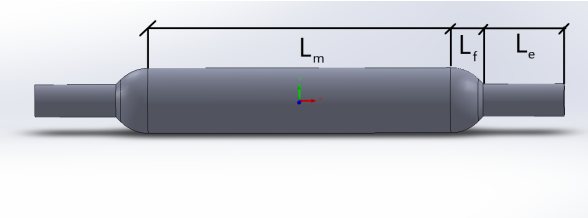

Figure 5.8: Model of mandrel with relevant lengths notated.

The lathe machining turned out to be difficult with such a long work piece. A slight misalignment between the head- and tailstock caused the mandrel to be turned with an eccentricity. The eccentricity was largest at the middle of the mandrel where the play was greatest. This manufacturing defect was not detected during quality control.

Demoulding was attempted when the filament winding of the first mandrel was complete. As the rudder stock was stuck to the mandrel it was attempted to freeze the part before extraction. This did not work and the rudder stock was destroyed during the extraction process as seen in figure 5.9.

Figure 5.9: Delamination from excessive force during attempted demoulding.

New Mandrel

A new mandrel was designed using the lessons learned from the first attempt. The mandrel part of the shaft was in this design a PP pipe with a outer diameter of 32 mm. The pipe was slid outside an aluminium shaft and connected to it with bolts, seen in figure 5.10. This was done to stiffen up the mandrel from the force of the filament winder.

There were several benefits to this design compared to the previous:

- A higher surface quality of the PP compared to the steel.
- An offer mandrel that could remain in the rudder stock of demoulding proved impossible.
- Quicker production time, as the PP pipe was bought, and the aluminium could be turned much quicker than steel.

Figure 5.10: PP pipe and inner aluminum shaft of mandrel.

The soft filleting wax, FILLWAX-330, was used to seal the small gaps around the edge of the PP pipe and the bolt hole, as can be seen in figure 5.11. As the epoxy resin doesn't stick to the wax this worked great as a seal and ensured that the bolt could be used to unfasten the PP pipe after the filament winding.

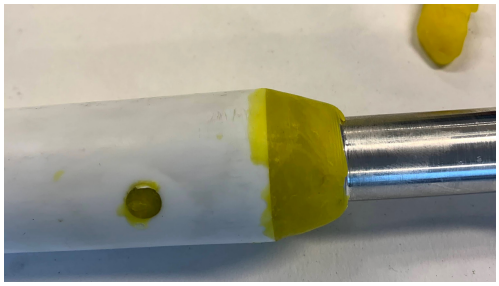

Figure 5.11: Delamination from excessive force during attempted demoulding.

5.3.3 Winding Parameters

The rudder stock was manufactured on a Mikrosan filament winding machine. The winding parameters are presented in table 5.5. The filament pretension was set to 20 N as the gals filament had a tendency of snapping if the tension was set any higher. This was suspected to happen as there was extra stress introduced thought friction and miss alignment in the pulley system.

Winding parameter	
Filament pretension	20 N
Winding time	2.3 h
Winding pattern	Helical
Curing time	48 h
Curing temperature	20^oC

Table 5.5: Winding parameters for filament winding.

The rudder stock was not post cured as the mandrel oven was out of service during production. This resulted in a longer curing time and lower structural properties. As the rudder stock had a wall thickness much higher than necessary, this was deemed acceptable.

The PP pipe was easily extracted from the aluminium shaft. During demoulding the PP pipe could not be extracted and was left in the rudder stock.

5.4 Hand Lay-up of Out-of-autoclave Prepreg

Hand lay-up of prepreg carbon fiber was used for the manufacturing of the skeg. This process was done mouldless and the prepreg was wrapped directly around the foam core and compacted using a vacuum bag. This was then cured in the oven, under vacuum, following the curing cycle recommended by the manufacturer. This manufacturing method was chosen based almost entirely on manufacturing time, as the machined foam core was delivered only days before the original project due date.

Hand lay-up of prepregs is normally an expensive process. It is also highly skill intensive and the results can vary much more than infusion type processes. The benefits to the prepreg system is the control over fiber fraction as the fibers are always perfectly impregnated. The process is also suitable for advanced geometries as the plys are sticky and can be moulded to 3D dimensional structures and even overhangs.

The high cost of the prepreg materials was not a factor for the skeg as the prepreg used was off cuts and rest material from Mark [39] project. The skill intensity of the prepreg process was underestimated when the manufacturing process was selected and the estimated time savings compared to a wet lay-up was not

achieved. The best process for the skeg manufacturing given the time constraints would have been a wet lay up using glass cloth.

5.4.1 Material Selection

The prepreg selected was used in Mark [39] project. It was a XC110 210g Twill 3k surface ply and XC110 416g Twill 6k backing ply. This choice was based mainly upon availability as it was left overs from a earlier project. The original out-life of the material was 28 days, but when it was used for the skeg it had only 15 days left. This was reduced to 13 days when the process was over and they were put back in the freezer.

The prepreg is a carbon fiber epoxy system that is designed for out of autoclave manufacturing. Its material properties and process guide can be found on the distributors web page [43].

The core material used was the *MyCell 80kg* PVC foam. This is the same core material as was used in the rudder and is described in section 5.2. This foam has a maximum service temperature of 180^oC and is advertised as being compatible with high temperature curing cycles. Maximum curing temperature needed for the XC110 system was 120^oC this was deemed acceptable.

5.4.2 Lay-up

The lay-up process was done by following the steps presented in the suppliers web page [43], and accompanying informational video [44]. The process consisted of the following steps in chronologically order:

- Letting the prepreg defrost for one day.
- Using masking tape to measure the geometry of the templates.
- Flattening out the tape, and creating templates out of paper from the tape measurements.
- Cutting the prepreg using the paper templates.
- Placing the backing ply down on the core material. Great care is used to ensure contact between the ply and the core surface everywhere.
- When placing adjacent plys, ensure a sizable overlap to ensure strength.
- Repeat the previous two processes with the surface ply.
- Wrap the laminate in unperferated release film and breather, making sure it is thoroughly compacted into every detail of the part.
- Finally put the part in a vacuum bag and pull a full vacuum.

Through this process several problems and challenges arose. The first process challenge was that the backing ply did not adhere to the core material very well during lay-up. It had great adhesion to other objects however and had a tendency to get stuck together in folds and wrinkles. This combined by the inexperience of the manufacturer resulted in several surface defects and wrinkles in the part, particularly around the sharp corners of the bushing mounts, pictured in figure

5.12. Another problem area was the leading edge. Here the ply on each side of the edge stuck together creating a ridge on the leading edge.

To improve the prepreg lay-up process, the foam core could have been coated in a material the prepreg would have bonded to better. This would have had to be a high temperature polymer to survive the curing process of the prepreg.

Figure 5.12: Wrinkles and surface imperfections in skeg.

5.4.3 Curing

The standard curing cycle form the manufacturer was followed. As the oven at NTNU does not have temperature ramping control the switched version was used, depicted in figure 5.13.

Standard (Switched) (only for use when oven ramp control is not available)

Step #	Start Temp	Ramp Rate	Time	End Temp	Elapsed Time
1	~20°C	Full	N/A	70°C	00:00
2	70°C	Soak	04:50	70°C	04:50
3	70°C	Full	N/A	120°C	00:00
4	120°C	Soak	01:25	120°C	06:15
5	120°C	Natural Cool	--	~20°C	07:15

Figure 5.13: Curing cycle from XPREG [43].

A vacuum was pulled on the part the entire time by threading a vacuum tube through the venting hole of the oven. The oven at the polymer and composite lab at NTNU has bad temperature control and the temperature often varied $\pm 5^{o}C$ around the set temperature. This is not expected to impact the performance of the composite significantly but is worth noting, as temperature control is very important for advanced composite manufacturing.

The worst of the surface defects were so big that they were sanded down all the way down to the core, and carbon cloth was used to patch over the imperfections with a wet lay-up. To a overlap of 50mm was used when patching during the post processing.

5.5 Adhesive Bonding

Adhesive bonding is a necessary composite manufacturing technique in many cases. As it is often impossible to make the entire part in just one mould. As all the composites made during this project was epoxy based so a fast curing epoxy was used as the adhesive. This was either a special adhesive epoxy or the RIMR135 epoxy system used in the infusion processes and filament winding.

An adhesive bond was used to fasten the flange to the skeg and to assemble the rudder before the mouldless VARTM. The adhesive bonding consisted of the initial bonding using the fast curing epoxy and later using a wet lay-up with glass fiber cloth to reinforce the joint. The strength of the adhesive bond was not explored during the design phase.

5.5.1 Rudder bonding

The rudder design relied on a large amount of adhesive bonds. The four parts of the spoke was glued to the rudder stock, and the foam core was later glued on to the resulting structure. The bond between the stock and the spokes was critical as it would transmit the majority of the torque.

Before the bonding could start it was essential that the three NACA profiles of the spoke was aligned. This was done by 3D printing a support where the underside of the profile was placed, providing a level base. A bubble level was then used to ensure alignment.

Once properly placed, the spoke was glued to the rudder stock in small sections, much like spot welding. This provided a rigid structure to work with while reinforcing the joints. The Saertex X-E-302g/m^2 fiber cloth and RIMR135 epoxy was used to reinforce the joint. The fastest hardener RIMH134 was used to speed up production time.

The cloth was impregnated and then tacked onto the joint with good overlap on both sides. If the space was available an overlap of 30mm was used. For the joint between the rudder stock and the spoke plate one continues fiber strip was used to join the two parts, wrapping around the stock to bond to both sides of the plate. This reinforcement can be seen in figure 5.14.

The RIMR135 system is a low viscosity epoxy and is therefore quite runny during the wet lay-up. The solution the author used was to wait 15 minutes after mixing in the hardener for the right viscosity during bonding.

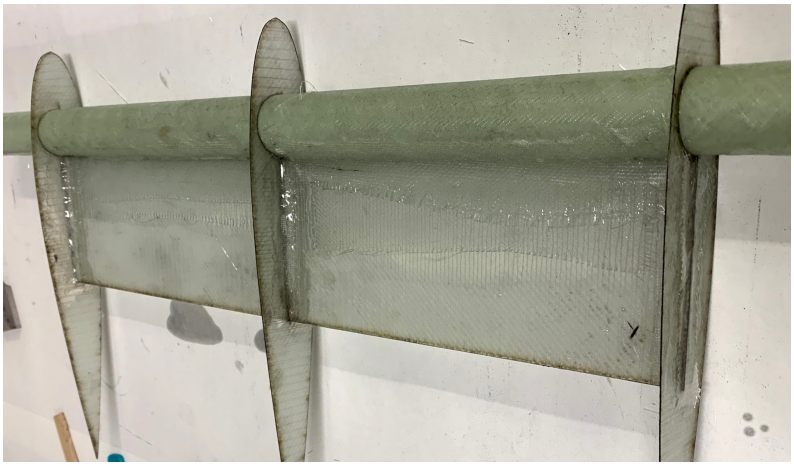

Figure 5.14: The rudder stock and spokes during adhesive bonding.

The core was bonded to the internal structure of the rudder with the RIMR135 system and the fast hardener. The areas to be bonded was coated in the resin and the foam core was the clamped down in position during curing. An example of the clamping used can be seen in figure 5.15.

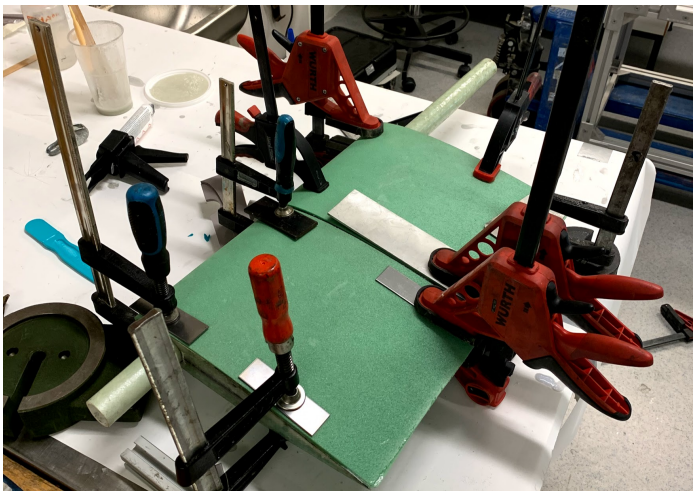

Figure 5.15: Clamping used during the bonding of rudder core.

5.5.2 Skeg Flange bonding

The adhesive bond of the skeg was critical in both a strength and positioning aspect. This bond would transfer all the bending moment the skeg experiences to the flange. This bond would also fix the positioning of the skeg relative to the hull and a slight misalignment could result in lift forces being generated by the skeg while to vessel was going straight introducing a constant turning force.

A rig, depicted in figure 5.16, was made to align the skeg and flange. This was made up of rigid aluminium profiles and clamped down on the flange. The position of the skeg was then adjusted until it was equally spaced between the two columns. This method was pretty accurate as a small misalignment at the base resulted in a big change at the top.
This measurement method did assume that the two sides of the skeg was symmetrical, and that the skeg flange was accurately cut, something that might not necessarily be true.

Figure 5.16: Rig made to measure skeg misalignment.

The top of the skeg was bonded to the flange with the fast acting bonding epoxy. The areas to be bonded was coated with the epoxy and clamped together in a similar way to the rudder in fig 5.15. The joint was reinforced on the outside using the same glass fiber cloth and epoxy system as used on the rudder 5.5.1. The same methodology and minimum overlap was also used as on the rudder.

5.6 3D Printing

The fast iteration possibility and ease of prototyping was the reasoning behind using a 3D printer to make the plastic gliders, rudder spacer, and profile support. None of the parts had any substantial loading and had tricky geometries that would have been hard to produce using conventional manufacturing methods.

An *Original prusa i3 mk3s* 3D printer was used for all 3D prints. The same printing parameters were used for all parts, and can be seen in table 5.6.

Printing parameters	
Material	PETG
Nozzle size	0.6
Layer height	0.35
Infill	10%

Table 5.6: 3D printing parameters.

These printing parameters where chosen to prioritize printing speed as both the support and the glider went through multiple iterations before the design was finalized.

The profile support was too long for the 3D printer base so the design was split in two and a snap connection was designed and integrated as a part of the print, shown in figure 5.17. This made it possible to print 4 profile supports per print, and the print time was 6 hours and 35 minutes.

The storage gliders were much smaller and was printed in batches of 16. The print time of the gliders was 4 hours and 49 minutes.

The lever arm spacer was only printed once, and had a print time of 1 hour and 15 minutes.

Figure 5.17: 3D printed profile support with snap connection.

5.7 Post Processing

Post processing is an unavoidable necessity during composite manufacturing. There are many forms of post processing methods as described in section 2.5. In table 5.7 an overview of which parts were finished with the different methods is given.

		Conventional machining	Laser cutting	Abrasive water-jet cutting
Hull	Storage tray	x		x
	Section partitions	x		x
Rudder	Rudder stock	x		
	Spokes		x	
	Finished Rudder	x		
Skeg	Flange	x		
	Shell	x		

Table 5.7: Overview of post processing methods used.

The storage trays and blind flange was cut out by the laminate plate by AWJ cutting. These parts fitted the AWJprocess well as they had a relatively big wall thickness of 3mm and wholes were required to be placed with precision on the surface of the plates. The AWJ cutting was done by workshop personnel and they used an algorithm that placed the initial insertion into the material away from the finished surface. This resulted in a good result with practically no delamination or fraying. The bolt holes made by the AWJ were unfortunately a bit uneven and often a bit undersized, so the where finished up with a manual drill.

The rudder spokes were cut out of their plate using laser cutting. As the plate was small and thin, with only a thickness of 0.9mm, it was decided that the heat affected zone would not be large and that the parts would not be compromised. The laser was set to full power and cutting speed was set to the preset for glass of 2mm. The laser was able to cut through the composite without problems. The only visible damage to the parts from the laser cutting process was a slight discoloration around the edges. This is likely epoxy over curing and degradation from the heat of the laser. This edge discoloration was very local and was only found in a radius $<$ thickness of the part around the cut. This gives confidence in that the heat affected zone was appropriately small.

The conventional cutting tool used for cutting and trimming was a rotary Dremel. An electrical $Dremel 4000 High Performance Variable Speed Rotary Tool$ was used for the glass fiber and a air pressure driven rotary tool was used for the carbon fiber as to not destroy the electronics with carbon fiber dust. The rotary speed was set to maximum, $35,000 RPM$ for the Dremel 4000. The feed rate was attempted to be as low as possible, but process control was hard with a hand held tool. The cutting tool used was a thin abrasive cutting disk made out of diamond grit. These steps was to minimize defects during machining as described in section 2.5.

5.8 Manufacturing of Non-composite Components

Table 5.8 summarises the manufacturing of the various non-composite parts done during the project. It states which method was used, who performed the operation, and comments on the process and results. All the parts were made out of AISI 316L stainless steel and was to be used in the rudder actuation system.

Component	**Method**	**Performed by**	**Comments**
Rudder actuator fastener	Turning + drilling	A.V.B	Turning process went well, achieved high tolerances between the fastener and the actuator.
Lever Arm	AWJ cutting	Workshop personnel	Very quick and gave good results. The internal holes had to be sanded down afterwards.
Rudder shaft	Turning + milling	A.V.B	The turning process went well with diameter tolerances of about $\pm 10\mu m$. The milling was done a bit too deep and resulted in slack between the shaft and the lever arms. Solution: weld the lever arms to the shaft.
Rudder actuator pin	Turning + drilling	A.V.B	Both turning and drilling resulted in a good quality part.

Table 5.8: Overview of manufacturing of non-composite components.

5.9 Hull Assembly

The hull assembly consisted of four pipe sections, connected with a bolted internal flange sealed with an O-ring. Between the sections was a blind flange to complete the partitioning of the hull and also to make up the combined seal between the sections. Five separate joints had to be assembled; three joints connecting the pipe sections and two lids at either end. An overview of the hull joints and their numeration is shown in figure 5.18. The full machine drawings for the pipe sections can be found in Appendix A.

The pipe sections had several production quality issues and design flaws that made the assembly process difficult. These problems consisted of deformations in the pipe sections, small bolt grooves for the internal flange, and inconsistent O-ring housing machining. These inconsistencies resulted in the assembly process taking approximately 4 hours. Ideally this should be done with two operators, as the pipe sections have a significant weight.

5.9.1 Deformations in the Pipes

There was sever deformations in the edges of the pipe sections. These made it very hard to align the bolt holes from one section to another. None of the pipe

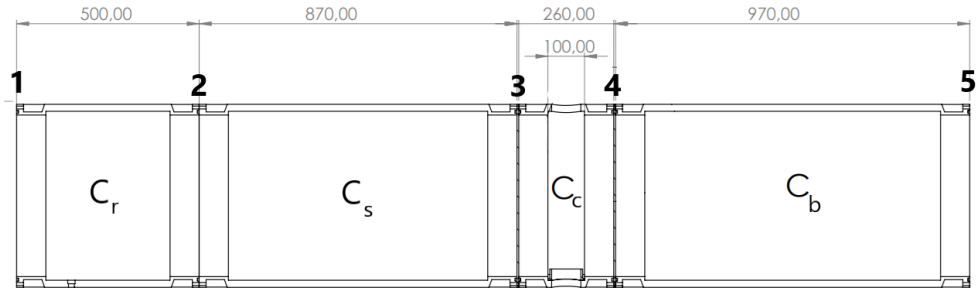

Figure 5.18: Assembly drawing of hull with compartments and connections annotated. C_r is rudder compartment, C_s is stern compartment, C_c is midpoint connection compartment, and C_b is bow compartment.

edges were perfectly circular and they were all deformed in unique ways. The pipe misalignment can be seen in figure 5.19.

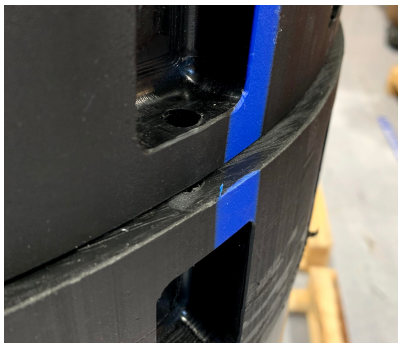

Figure 5.19: Deformation of pipe edges, resulting in big gaps between bolt holes.

This deformation made it hard to mount the GFRP blind flanges in joint 1 and 5, as notated in 5.18, as the lids had been AWJ cut to the exact hole placement. This was fixed by enlarging the holes in the lids.

The deformation in the pipe connections made joints 2,3, and 4 even harder to close. The pipe sections were rotated relative to each other and every hole configuration had to be checked to find the best fitting match. This was done by finding the biggest bolt hole misalignment and minimizing this. The best fit between sections was marked with a tape strip.

The bolts were then forced through the pared holes and/or bolt holes were widened if necessary. The force required to put the pipe sections together caused new small deformations in the material around the bolts.

The deformation of the pipe sections was probably caused by the release of residual stresses during cutting as described in section 3.1.

5.9.2 Small Bolt Grooves

The bolt grooves, depicted in figure 5.20, was too narrow and shallow, so that an electrical drill, or a ratchet, could not be used to fasten the bolts. Instead all bolts had to be fastened by hand with a wrench, increasing assembly time significantly and with litle moment control on the bolts.

Figure 5.20: Bolt connection in hull bolt groove visible.

A solution to this problem would be to machine the slots to a larger size. This could not be done at this stage due to the fast approaching master project deadline.

5.9.3 Inconsistent O-ring housing

The O-ring housing on the flange face was machined at variable distance from the inner pipe surface. The designed distance between the O-ring housing and the inner wall of the pipe was 4.4mm as shown in figure 5.21. When the pipe parts arrived this distance had very bad tolerances, and varied ±2mm.

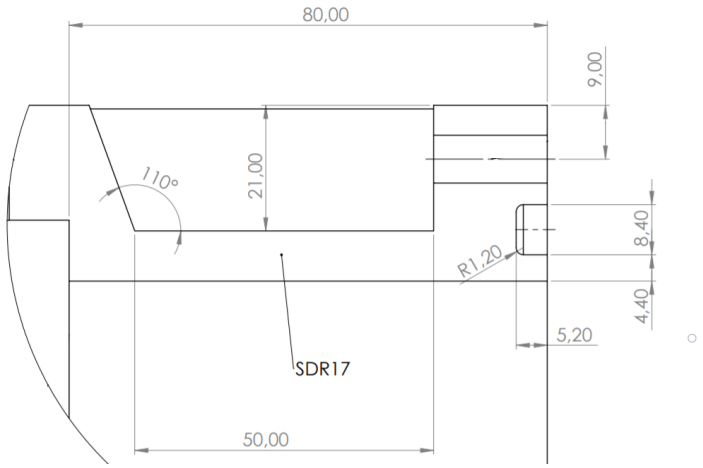

Figure 5.21: Excerpt from detail drawing of pipe connection.

This made the O-ring come dangerously close to the bolt holes, and the inner sidewall, and made it hard to achieve an even compression on the o-ring, thus

securing the connection against leakage.

This manufacturing flaw was significantly outside of the specifications sent to Astorplast, who produced the flanges. This would normally be grounds for a complaint, and new parts could be expected to be delivered free of charge or at a reduced price. However, the claim might be weakened, as the drawings sent to the producers did not include tolerances.

The complaint was not made to the manufacturer, but might be something to consider in the continuation of the ORCA project.

5.10 Rudder System Assembly

The rudder assembly contained three separate system designs; the rudder, the skeg, and the actuation system.

The bearing on the top of the skeg was slid down the rudder stock. The rudder was then slotted down into the lowest bearing and the bearing on the top was then fastened to its housing in the skeg using a strip brace. The fastening method is depicted in figure 5.22.

Figure 5.22: The rudder fastened to the skeg using a galvaniced steel strip brace.

The skeg was mounted to the hull with 8 M8 bolts. These bolts were connected to metal inserts described in section 4.1.4. These inserts were threaded using a pilot hole of 10.3mm.

The aluminium profiles for the tray were fastened to the inside of the rudder compartment of the hull using M6 bolts and ditto inserts to the pipe wall. These inserts were hard to mount, as the available space just barely fitted the drill needed for the operation.

After the aluminium rails were secured, the tray containing the rudder actuation system was inserted. The linear actuator mount and the ball bearing were bolted to the tray in holes cut by the AWJ. There were no additional adjustments needed. The rudder was slid over the steel shaft. A bolted connection was sup-

posed to fasten the shaft to the stock, but this proved not to be possible within the master project time frame. The full system assembly is shown in figure 5.23.

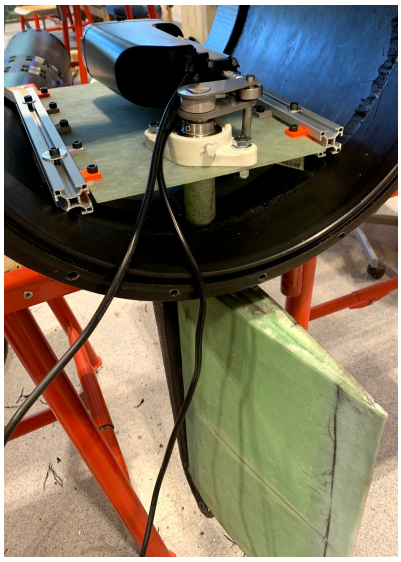

Figure 5.23: The rudder system fully assembled.

5.11 Estimated Cost

One of the main design principals, during design and manufacturing of the hull and rudder, was to minimize cost. Table 5.9 shows confirmed material costs including the cost of every new part that was bought especially for this project.

Part	cost[NOK] / unit	Amount	Cost [NOK]
PE hull	11872.5	4	47490
O-rings	1250	14	17500
M6 inserts	17.0	50	848
M8 inserts	14.8	50	739.8
Polymer bushings	73.7	2	147.4
Stainless bearing	750	1	750
PVC foam	2696	1	2696
Sum			70,171

Table 5.9: Cost of bought parts and material.

Table 5.11 includes fibers and resin materials used during the project. Exact measurements were made of resin and fiber used during VARTM and mouldless VARTM, shown in table 5.2, and table 5.3. The amount of prepreg used during

Product	cost[NOK] / unit	Amount	Cost [NOK]
Sticky tape	2.46 / m	21.7	53
Flow mesh	12.3 / m^2	2.8	34
Vacuum bag	12.3 / m^2	4.8	59
Vacuum tube	6.2 / m	24	149
T-piece	6.2	11	68
Peel ply	16 / m^2	3.2	51
Spiral tube	2.5 / m	3.8	9.5
Sum			424

Table 5.10: Consumables used during project.

the hand lay-up was estimated by calculating the surface area of the skeg. In reality more material was used, as the calculation did not account for the overlap between sections during lay-up.

Prices used in table 5.11 were retrieved from the manufacturers and converted into NOK at the appropriate rate in August 05 2021. As the manufacturer and product name could not be found for the "generic E-glass" an estimated cost of $30 NOK/m^2$ was used. The price of HiPerTex W2020 could not be found, but by comparing several similar filament wound rolls, a price of $20 NOK/kg$ was estimated. The price of the epoxy systems used, varies depending on quantity and market demand. At the last purchase, the price was close to $100 NOK/kg$, and this number is used in the budget calculations.

Product	cost[NOK] / unit	Amount	Cost [NOK]
200g 2x2 Twill woven	24.8 / m^2	0.6	15
Saertex X-E-302g/m^2	23.7 / m^2	0.6	14
Generic E-glass	30 / m^2	6.6	198
MGS RIMRI135 epoxy system	100 / kg	16.4	1640
XC110 210g Twill 3k	383 / m^2	0.21	80.43
XC110 416g Twill 6k	416 / m^2	0.21	87.36
HiPerTex W2020	20 / kg	0.2	4
Sum			2039

Table 5.11: Fibers and resin used during production.

The consumables in table 5.10 were used in VARTM, mouldless VARTM, and the hand layup process. Prices are retrieved from *easycomposites.co.uk*. The consumable amount used during the project is approximated by assuming a 50mm

gap between the end of the fiber and the vacuum bag in the VARTM process. For the other two processes a rough estimate was made for the size of the vacuum bag.

The total material cost for the construction of a hull and rudder was

$$C_m = 72,634NOK. \tag{5.2}$$

Where the vast majority, 97% of the cost, was related to the hull production. The freight cost is not included in any of the cost calculations.

There is normally a significant difference between manufacturing time for a prototype and manufacturing time when production method is set. This will also impact the estimated manufacturing cost. In table 5.12, development time and estimated optimized production time is presented. To calculate production cost, a flat rate of $500NOK/h$ was used. Only composite manufacturing was analysed in the manufacturing time calculations. These processes contain the production off all composite parts.

Process	**Real manufacturing time [h]**	**Optimized manufacturing time [h]**
VARTM	30	15
Mouldless VARTM	9	4
Filament winding	50	4
Hand lay-up	10	8
Post processing	40	8
Adhesive bonding	20	8
Assembly	30	6
Sum	189	45
Sum cost	94,500	22,500

Table 5.12: Comparison and calculated of manufacturing time and cost.

It is estimated the an ideal filament winding process could cut production time significantly. This process should normally be quite efficient once a working mandrel and winding program are set up. The process time for the other manufacturing methods could be reduced by avoiding mistakes during manufacturing and also running multiple processes simultaneously.

The hand lay-up process, however, can not be optimized much, as the curing cycle requires monitoring when using the oven at NTNU.

The total cost of hull and rudder is estimated to be

$$C = 72,634 + 22,500 = 95,5134NOK, \tag{5.3}$$

if the production was optimization as discussed above.

Chapter 6

Experiments and Testing

Two test were done on the parts produced during this project. The hull was subjected to a waterproof test, to test the joints between the pipe sections. This was an initial test before any apparatuses could be installed and a sea trial could be conducted.

The rudder was subjected to a dry system test where the rudder, hull, and actuator system was assembled and the rudder was actuated. This test was a prerequisite to a planed deflection and stress test to be done later. This later test was never done due to time limitations.

6.1 Waterproof Testing of Hull

Having a watertight hull is a prerequisite to having a working vessel. This property of the hull supersedes any of the design goals, table 1.3, as the hull does not function without it.

6.1.1 Experimental Setup and Method

The five pipe connections were tested separately. Each pipe section was filled with water to a height of 500 mm, thus simulating the water pressure experienced by the vessel being fully submerged. The pipes were left submerged for two hours and visually inspected for any leakages. Figure 6.1 shows one of the pip connections under testing.

The bolts in the connection were tightened by wrench as a torque measuring ratchet did not fit in the bolt groove. All bolts were tightened to the same - to the best of the authors ability.

If a leakage was detected every bolt in the connection was further tightened and the test would start again. A maximum number of three tightening cycles were performed.

Figure 6.1: Joint 3 under waterproof test.

6.1.2 Results

Table 6.1 shows the results of the waterproof test. The joints in the table are numerated according to the naming convention established in figure 5.18.

Joint	Leakage	Comment
1	-	Tightened 2 times
2	2 spots with small waterdrops	Tightened 3 times
3	2 spots with small waterdrops	Tightened 3 times
4	5 spots with small waterdrops	Tightened 3 times
5	-	Tightened 1 time

Table 6.1: Results from waterproof test.

A picture of a leakage during the test can be seen in figure 6.2.

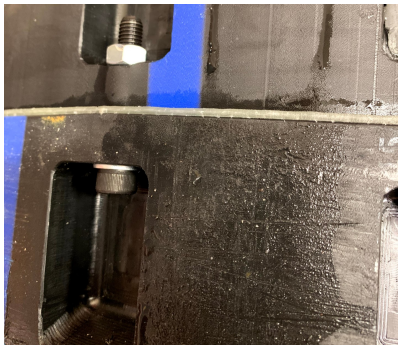

Figure 6.2: Joint 3 under waterproof test.

6.2 Rudder Assembly actuation test

The rudder actuation test was a quick test to see if the actuation system worked and could rotate the rudder without to much friction.

6.2.1 Experimental Setup and Method

The setup for this test was the assembly of the rudder system described in section 5.10. The LA33 linear actuator was powered by a 24V DC power supply unit. During the test the actuator was controlled manually without feedback. The assembly is shown during testing in figure 6.3.

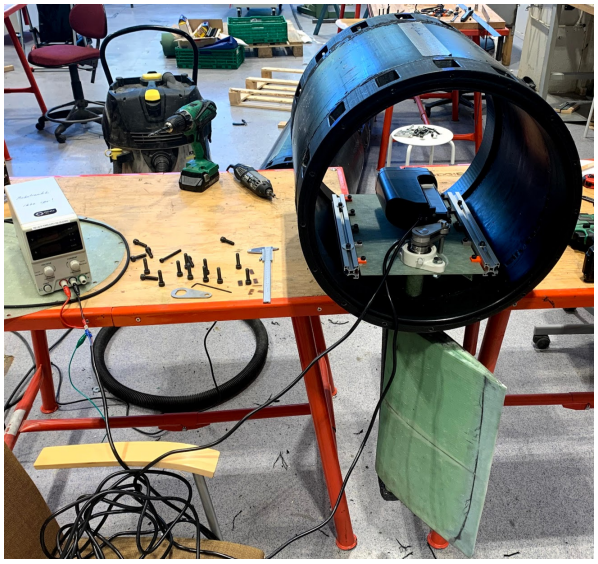

Figure 6.3: The full rudder assembly during testing.

6.2.2 Results

The rudder actuation system worked. The LA33 moved the rudder back and forth the 60^o the system was designed to. There seemed to be a bit of friction in the tight hole where the rudder stock penetrated the hull (the shaft seal was not mounted in this assembly), but the actuator did not seem affected.

The exact position of the rudder was very hard to control manually. The system also lacked a digital stop to prevent the linear actuator from extending beyond the maximum intended range.

Chapter 7

Discussion

This chapter discusses the design and production of the hull and rudder of the ORCA prototype. The different elements in the prototyping process will be compared to the research objectives stated in section 1.5.

7.1 Design

7.1.1 Hull

The hull, as it stands, is not waterproof. This is equal to a hull failure and renders the prototype unusable for practical tests. Any benefits a modular hull design, made by a readily available pipe material, does not come into affect until the hull functions as a hull. Several aspects of the hull design contributed to the failed seals in section 2,3, and 4 as seen in table 6.1.

Basic Design

The basic design of the hull was decided in the project thesis and at start-up of the master thesis. The prerequisites given included the hull being made out of pipe sections instead of a traditional GFRP hull. The benefits to such a design includes its modular nature, and ability to quickly be customized to different sections and lengths depending on the mission. The design also allows for the hull to change lengths during prototyping to find the right center of pressure from the sail relative to the hull. A drawback to the design, that was not fully taken into account at the time, was that a pipe section design necessitates the section seals to be under water at all times. A traditional vessel design, with lids on top, does not have this continuous stress. A minor leakage would not necessarily result in failure, and also the water pressure on the lid seal would be minimal in most cases.

An other oversight in the initial design criteria was the allowance of a single point of failure in the pipe joints. If one bolt or o-ring were to fail, the seal would not be watertight anymore. The introduction of such a failure criteria would have

necessitated a more rigid design, and probably increased weight. The top design goal of the hull was durability, and such a single point of failure criteria supports this goal.

Material selection

PE was used for the pipe material as it is commonly available and standardized in pressure pipes with the right outer diameter. PE is also a ductile material compared to PVC, giving it better impact resistance. PVC have benefits over PE as it has a higher strength and stiffness, resulting in higher form stability. This would have made the joint design and construction easier. PVC becomes too brittle at lower temperatures and was therefore rejected as a pipe material. If the specified temperature range for the vessel had been higher, PVC might have been an attractive solution.

Another added benefit with PVC is the possibility of using adhesive bonding. This does not work with PE as adhesives does not stick to the material. This would have made all the elaborate insert and bolt connections unnecessary.

PE has great properties for all the parts of the hull except the connection points and penetration points, where a stiff and form-stable construction is needed. It might be possible to address these material weaknesses, by adding stiffness to the construction using a combination of other materials.

- PE alone is not suitable for flange designs during movement.

-PE hull would have been suitable for a welded design or a "kayak" design - where the hull is molded in one piece.

Pipe connections

The internal flange pipe connection was a novel idea. The design contains benefits from a traditional flange design, but without the hydrodynamic drag. The drawbacks are the uncertainties that comes with a new design as well as the need for specialized machining. A new design can not use stock parts as a normal flange would have.

A possible way to stiffen up the pipe connection is to increase the wall thickness in the connection. The pipe section chosen was SDR17, with a wall thickness of $29.7mm$. This design fulfilled the design criteria to minimize weight. The weight saving was prioritized, as pipe sections should be light enough for one person to carry. If the thicker pipe class of SDR11 had been chosen this would have added $3.3kg$ to every pipe section. One extra benefit of a SDR11 pipe section at the joint, is the extra room it would give the O-ring housing. This would have made it possible to placed the o-ring with better tolerances, away from bolt holes and the inner side wall, making the design more robust against manufacturing flaws.

Another possibility of stiffening the connection between pipe sections, not explored in this report, is to insert steel sheets, as blind flange material, on the butt of every pipe. This metal plate would then be the one to compress an O-ring seal.

The surface quality of the blind flanges might have contributed to the leakages. The VARTM process does not produce good surface quality on both sides of the part and the blind flanges needs to seal on both ends in section 2,3, and 4. If the post processing of these blind flanges did not result in good surface quality, this could cause a leakage. The surface quality of the blind flanges are unknown as it was not measured.

The assembly process of the pipes were manageable by one operator. However, the assembly was difficult with regard to bolt tightening as the grooves where a bit narrow. With wider groves, as described in section 5.9.2, the bolt tightening process would be smother as well as making it possible to tighten the bolts with higher precision.

Internal Storage Trays

An internal storage system based on modular trays were designed and manufactured for the pipe hull. The trays were easy to assemble as they slotted into aluminium rails. While the storage trays were manufactured as flat sheets, the can easily be modified or replaced with new tray designs. The only limitation being the fixed width between the rails. This flexibility allows for the further customizability of the ORCA vessel to a specific mission or sensor pay load.

7.1.2 Rudder

An original rudder design was developed and manufactured during this project. The system was shown to function from the assembly actuation test, but further mechanical and functional tests need to be conducted on the rudder to asses the designs suitability. The functional tests will, for practical reasons, need a working hull to be completed.

Bearing design

The bearings used between the rudder and the skeg were polymer bushings. These are cheap bearings compared to stainless steel ball bearings. They also have superior corrosion resistance. Thus following design goal 1 and 2: durability and cost.

As a trade off for corrosion resistance comes erosion resistance. Small particles could come between the rudder stock and the bushings and over time erode the parts. The erosion rate is unknown, but expected to be slow. Anyhow, wear and tear will have to be monitored and serviced when the vessel is in for service.

Impact resistance of rudder

A study on impact resistance of the rudder system was not done. As impact protection of the rudder is one of the skeg's functions, this is a missing part in the design analysis. During a long mission a vessel might encounter drift wood, icebergs or other objects that could impact the rudder.

The skeg was designed with the bending moment from the hydrodynamic forces as the critical load. This resulted in a design with a strong flange, but with a relatively thin shell everywhere else. This thin shell might not be suitable during a possible impact.

Actuator design

The rudder actuator system designed was functional. The LA33 actuator worked according to specifications and rotated the shaft without problems. All parts in the design are made of the same stainless steel alloy for corrosion resistance. The metal parts were also relatively easy to manufacture and had good tolerances. Some play in the system was found, but this is due to the lever arms being loosely fitted to the shaft, and could easily be fixed by welding the connection.

The manual actuator control, without feedback, worked well for the limited testing in this theses, but a more complex controlling system must be developed for the final set-up.

Design for manufacturing

The rudder system was for the most part designed almost parallel with production. In this way a feedback loop influenced the design process in a way suitable for a prototype design production process.

One example of good design for manufacturing, was the rudder spokes. A spoke design made of flat sheets, assembled as puzzle pieces, made for a fast and easy construction.

7.2 Production

7.2.1 Hull

The production of the hull was handled by a contracted manufacturer, Astorplast. The pipe parts delivered were deformed and had machining flaws. These flaws are most likely the reason why connection 2,3, and 4 could not be made watertight. These manufacturing flaws are at scale that a claim for re-fabrication might be warranted. One factor weakening a claim is the lack of tolerances given on the machining specification drawings.

The decision to have a third party manufacturer do the pipe construction does have its positives. A mirror weld is preferably used when welding pipe sections

as it is faster and results in a stronger weld. NTNU does not have access to mirror welding equipment. The machining of the O-ring housing requires tight tolerances. This should be easier to achieve using machines especially set up for machining PE. The outer diameter of the pipes used is also to large for the lathes and milling machines at NTNU. Also, bringing inn a third party in the production, opened up insight on design as experienced machining operators had their own ideas related to what was practical to machine and towards functionality of design.

The drawback with having the pipe parts produced by Astorplast were costs. The construction of the pipes stood for 65% of the total production costs. As this dramatically cut down on production time however, the trade off might be acceptable.

7.2.2 VARTM

- The VARTM process was only used to produce simple GFRP parts. All the parts turned out with acceptable quality with no visible voids or dry spots. The strength of the VARTM process is its repeatability and consistency compared to hand-lay-up of prepregs of wet laminates. The VARTM process can be a fast and efficient production method for planar or slightly curved sheets. These parts does not need a specially designed mould, which greatly reduces production time. The cost of the VARTM was also kept low as multiple parts were made from the same sheet, reducing the consumables needed.

7.2.3 Mouldless-VARTM

The mouldless-VARTM was cost effective process for prototyping. The process effectively built the mould and part at the same time. Cutting production cost and time compared to normal VARTM. A slight decrease in quality is sighted as this poses the main down side to mouldless VARTM compared to normal VARTM. The surface quality from the mouldless-VARTM was similar to that of the peel ply side of the VARTM process, giving the surfaces a rough texture. This is to be expected as the fibers were wrapped in peel ply. The geometric tolerances of the infusion were good and no geometric deviation was detected. This indicate that the core material and internal GFRP structure of the rudder were strong enough to stop any warping during curing.

Using the mouldless-VARTM process might also have contributed to the construction strength. In a normal rudder production two shell halves are bonded together making one continues seam. In the mouldless-VARTM process the whole shell is placed as one strip of fiber and the overlap is bonded in the initial infusion process. This reduces the size of the joint and ensures a good bond.

Even though this process worked great for the construction of the prototype rudder, it is not recommended for mass production. The drawbacks of building a

mould diminishes as it can be reused for multiple parts.

7.2.4 Filament winding

The filament winding process produced a high quality rudder stock. This process had a high initial time investment, and maybe not be suitable for prototyping. Before the filament winding process can begin two time consuming processes must be done. Manufacturing a mandrel and programming the winding process. As seen in section 5.3.2, the mandrel is a critical part of the process and it needs to have a high quality surface finish and dimensional accuracy.

The new mandrel solution using an "offer mandrel" around a machined aluminium shaft represented a good solution. It saved a lot of time as the mandrel was not required to be machined to such high quality standards. An even faster production method would have been to make the rudder stock using hand lay-up. The hand lay-up could have been achieved using only the "offer mandrel" from the filament process and rolling it in glass fiber cloth. This would have saved a considerable amount of development and manufacturing time, but at the potential cost of material quality.

7.2.5 Hand Lay-up

Hand lay-up of prepreg carbon fiber was a relatively fast process and has the potential to produce high quality parts. The skeg's curvature and asymmetrical geometry made it hard to apply the sheets. The surface quality from the mouldless prepreg construction became quite rough. This due to deficient adhesion between the prepreg and the core material. The problems encountered may, to some parts at least, be contributed to the fitter's inexperience.

An alternative manufacturing process that could have been used was hand lay-up of wet fibers. This production method would have been similar to the prepreg variant in time and skill required, but would have cost significantly less. As the prepreg used in this case was left overs from an earlier project the cost aspect was not considered during prototyping.

Chapter 8

Conclusion

The objective of this master thesis was to design and manufacture a hull and rudder system for an ASV prototype. The two assemblies were to be designed and manufactured following the system design goals in table 1.3. The objective for hull was to explore the possibility of using polyethylene pipes to make a modular hull. The objective of the rudder was to produce a rudder system implementing efficient and fast prototyping manufacturing processes.

8.1 Hull

The pipe hull designed and assembled was not waterproof. It had leakages that could not be stopped in three of the five pipe connections. This renders the hull unable to function until a fix can be made. Several factors have been discussed as a potential cause of the connection failure. The suspected causes include:

- A manufacturing defect in the O-ring housing from the supplier.
- A dimensional defect in the pipe butt caused by the release of residual stresses.
- Thigh tolerance around the O-ring groove.
- Poor surface quality of blind flange.

The high ductility and low form stability of the PE pipe is also of concern in the pipe joint. The pipe hull concept could be made to work if the connection faces could be made more rigid. The single point of failure criteria should also be considered included in the design.

Aside from the manufacturing flaws, it makes sens to make up the hull of machined pipe sections. It saves a lot on construction and development time. The rest of the hull design seems to be well designed and build, but needs further testing.

8.2 Rudder

A composite rudder prototype was designed. No metal parts were used outside the hull to reduce degradation of the system due to corrosion. The failure modes were analysed and the design was altered to best withstand these.

Most of the composite manufacturing techniques used during the construction of the rudder were well suited for prototyping and resulted in a good quality part. The mouldless-VARTM process used on the rudder showed great results for a prototyping production method.

One production method that did not work as needed for a prototyping process, was filament winding. It gave good results, but at too high production time cost, as it caused significant delays om completion time for the master theses. Hand lay-up of fiber cloths around a PE mandrel is suggested as a suitable replacement.

No structural or stress tests were performed. These must be done and compared to the FEA, to determine if the manufacturing methods produced the predicted results.

Bibliography

[1] R. Stelzer and K. Jafarmadar, 'History and recent developments in robotic sailing,' in *Robotic sailing*, Springer, 2011, pp. 3–23.

[2] M. Neal, 'A hardware proof of concept of a sailing robot for ocean observation,' *IEEE Journal of Oceanic Engineering*, vol. 31, no. 2, pp. 462–469, 2006.

[3] M. F. Silva, A. Friebe, B. Malheiro, P. Guedes, P. Ferreira and M. Waller, 'Rigid wing sailboats: A state of the art survey,' *Ocean Engineering*, vol. 187, p. 106 150, 2019.

[4] P. H. Miller, M. Hamlet and J. Rossman, 'Continuous improvements to usna sailbots for inshore racing and offshore voyaging,' in *Robotic Sailing 2012*, C. Sauzé and J. Finnis, Eds., Berlin, Heidelberg: Springer Berlin Heidelberg, 2013, pp. 49–60, ISBN: 978-3-642-33084-1.

[5] R. Gården Rovik, 'The concept development for designing an autonomous sailboat,' 2017.

[6] M. Dyrseth, 'Development and design of a wingsail for an autonomous surface vessel,' 2019.

[7] S. Gauden, 'Development and prototyping of an ocean going autonomous surface vessel for research applications,' 2020.

[8] A. Brandal, 'Development and design of an autonomus surface vessel,' 2020.

[9] R. Fragoudakis, *Strengths and Limitations of Traditional Theoretical Approaches to FRP Laminate Design against Failure, Engineering Failure Analysis*. Kary Thanapalan, 2019. DOI: 10.5772/intechopen.89729.

[10] R. F. Gibson, *Principles of composite material mechanics*. CRC press, 2016.

[11] M. Hinton, P. Soden and A.-S. Kaddour, *Failure criteria in fibre reinforced polymer composites: the world-wide failure exercise*. Elsevier, 2004.

[12] K.-T. Hsiao and D. Heider, 'Vacuum assisted resin transfer molding (vartm) in polymer matrix composites,' in *Manufacturing techniques for polymer matrix composites (PMCs)*, Elsevier, 2012, pp. 310–347.

[13] M. Abusrea and K. Arakawa, 'Enhanced tensile strength cfrp adhesive joint constructed from carbon fiber-reinforced plastic and dry carbon fiber laminates,' Jun. 2016.

[14] S. Van Oosterom, T. Allen, M. Battley and S. Bickerton, 'An objective comparison of common vacuum assisted resin infusion processes,' *Composites Part A: Applied Science and Manufacturing*, vol. 125, p. 105 528, 2019.

[15] E. Ruiz, V. Achim, S. Soukane, F. Trochu and J. Bréard, 'Optimization of injection flow rate to minimize micro/macro-voids formation in resin transfer molded composites,' *Composites Science and Technology*, vol. 66, no. 3, pp. 475–486, 2006, ISSN: 0266-3538. DOI: https://doi.org/10.1016/j.compscitech.2005.06.013. [Online]. Available: https://www.sciencedirect.com/science/article/pii/S026635380500223X.

[16] J. A. Maley, 'An investigation into low-cost manufacturing of carbon epoxy composites and a novel "mouldless" technique using the vacuum assisted resin transfer moulding (vartm) method.,' 2008.

[17] T. Centea, L. Grunenfelder and S. Nutt, 'A review of out-of-autoclave prepregs – material properties, process phenomena, and manufacturing considerations,' *Composites Part A: Applied Science and Manufacturing*, vol. 70, pp. 132–154, 2015, ISSN: 1359-835X. DOI: https://doi.org/10.1016/j.compositesa.2014.09.029. [Online]. Available: https://www.sciencedirect.com/science/article/pii/S1359835X14003108.

[18] S. Peters, *Composite Filament Winding*. ASM International, 2011, ISBN: 9781615038527. [Online]. Available: https://books.google.no/books?id=nciMwbQfymQC.

[19] M. Lossie and H. Van Brussel, 'Design principles in filament winding,' *Composites Manufacturing*, vol. 5, no. 1, pp. 5–13, 1994, ISSN: 0956-7143. DOI: https://doi.org/10.1016/0956-7143(94)90014-0. [Online]. Available: https://www.sciencedirect.com/science/article/pii/0956714394900140.

[20] R. Komanduri, 'Machining of fiber-reinforced composites,' *Machining Science and Technology*, vol. 1, no. 1, pp. 113–152, 1997. DOI: 10.1080/10940349708945641. eprint: https://doi.org/10.1080/10940349708945641. [Online]. Available: https://doi.org/10.1080/10940349708945641.

[21] R. Komanduri, B. Zhang and C. M. Vissa, 'Machining of fiber reinforced composites,' in *Processing and Manufacturing of Composite Materials*, vol. 112, Jan. 1991, pp. 1–36.

[22] B. Kavad, A. Pandey, M. Tadavi and H. Jakharia, 'A review paper on effects of drilling on glass fiber reinforced plastic,' *Procedia Technology*, vol. 14, pp. 457–464, 2014, 2nd International Conference on Innovations in Automation and Mechatronics Engineering, ICIAME 2014, ISSN: 2212-0173. DOI: https://doi.org/10.1016/j.protcy.2014.08.058. [Online]. Available: https://www.sciencedirect.com/science/article/pii/S2212017314000942.

[23] S. Abrate and D. Walton, 'Machining of composite materials. part ii: Non-traditional methods,' *Composites Manufacturing*, vol. 3, no. 2, pp. 85–94, 1992, ISSN: 0956-7143. DOI: https://doi.org/10.1016/0956-7143(92)90120-J. [Online]. Available: https://www.sciencedirect.com/science/article/pii/095671439290120J.

[24] A. Kazakov, 'An automated method for the measurement of residual stress in melt-extruded plastic pipes,' *Polymer Testing*, vol. 17, no. 6, pp. 443–450, 1998, ISSN: 0142-9418. DOI: https://doi.org/10.1016/S0142-9418(97)00069-X. [Online]. Available: https://www.sciencedirect.com/science/article/pii/S014294189700069X.

[25] J. Poduška, P. Hutař, J. Kučera, A. Frank, J. Sadílek, G. Pinter and L. Náhlík, 'Residual stress in polyethylene pipes,' *Polymer Testing*, vol. 54, pp. 288–295, 2016, ISSN: 0142-9418. DOI: https://doi.org/10.1016/j.polymertesting.2016.07.017. [Online]. Available: https://www.sciencedirect.com/science/article/pii/S0142941816304512.

[26] M. M. Belaziz Azzeddine, 'Experimental study of the weld bead zones of a high-density polyethylene pipe (hdpe),' *Journal of Failure Analysis and Prevention*, vol. 18, pp. 667–676, 2018. DOI: https://doi.org/10.1007/s11668-018-0462-0.

[27] O. Balkan, H. Demirer and H. Yıldırım, 'Morphological and mechanical properties of hot gas welded pe, pp and pvc sheets,' *Journal of achievements in materials and manufacturing engineering*, vol. 31, pp. 60–70, 2008.

[28] 'Fluid power systems – O-rings – Part 2: Housing dimensions for general applications,' International Organization for Standardization, Geneva, CH, Standard, Aug. 2016.

[29] (), [Online]. Available: https://www.technifast.co.uk/threaded-inserts (visited on 02/04/2021).

[30] D. Casey. (), [Online]. Available: https://www.sailmagazine.com/diy/know-your-rudder (visited on 04/03/2021).

[31] N. K. Kar, 'Failure analysis of a composite rudder stock using 3d x-ray micro-computed tomography,' *Journal of Failure Analysis and Prevention*, vol. 19, pp. 24–28, 2019. DOI: https://doi.org/10.1007/s11668-019-00601-5.

[32] J. Liu and R. Hekkenberg, 'Sixty years of research on ship rudders: Effects of design choices on rudder performance,' *Ships and Offshore Structures*, vol. 12, no. 4, pp. 495–512, 2017. DOI: 10.1080/17445302.2016.1178205. [Online]. Available: https://doi.org/10.1080/17445302.2016.1178205.

[33] 'Rules for classification - ships - part 3: Hull, chapert 14: Rudder and steering,' International Organization for Standardization, Geneva, CH, Standard, Oct. 2015.

[34] (), [Online]. Available: https://jefa.dk/products/rudder-stocks/ (visited on 06/03/2021).

[35] A. Echtermeyer, K. Lasn and S. Shchebetov, 'Typical static ply properties for composites,' 2013.

[36] K. Lasn, A. Klauson and A. Echtermeyer, 'Back-calculation of elastic moduli of a ply from the moduli of cross-ply laminates,' *Mechanics of Composite Materials*, vol. 51, no. 1, pp. 55–68, 2015.

[37] (), [Online]. Available: http://www.caliberyacht.com/Features_Seaworthy_Detail_Rudder_Skeg_Stalling.htm (visited on 02/06/2021).

[38] R. E. E. E. Larsson, *Principles of Yacht Design*, 2nd ed. Adlard Coles Nautical, 2011.

[39] L. Mark, 'Design and fabrication of a passively adaptive carbon fiber propeller,' 2020.

[40] (), [Online]. Available: https://www.shaftseal.com/pss-rudder-seal.html (visited on 06/06/2021).

[41] (), [Online]. Available: https://www.metyx.com/wp-content/uploads/PDF_Files/Hexion/TDS/TDS%5C%20RIMH%5C%20137.pdf.

[42] E. Greene *et al.*, 'Design guide for marine applications of composites,' Ship Structure Committee, Tech. Rep., 1997.

[43] (), [Online]. Available: https://www.easycomposites.co.uk/xc110-416g-22-twill-6k-prepreg-carbon-fibre.

[44] (), [Online]. Available: https://www.youtube.com/watch?v=HfrFaKDsJxc (visited on 06/08/2021).

Appendix A

Machine drawings

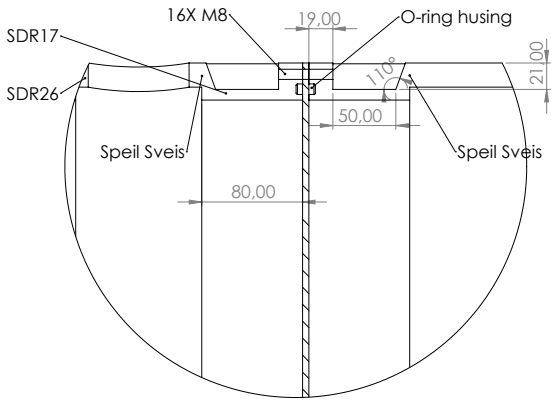

DETAIL C

SCALE 1 : 3

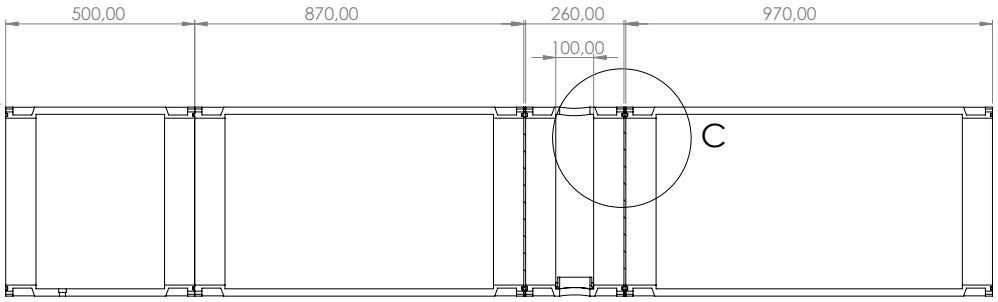

SECTION A-A

SCALE 1 : 10

ITEM NO.	PART NUMBER	DESCRIPTION	QTY.
1	Midt rør, 260	Har O-ring husing på begge ender	1
2	Front rør, 970	Har O-ring husing på begge ender	1
3	Bak rør, 870	Har O-ring husing på 1 ender	1
4	Ror-rør, 500	Har O-ring husing på begge ender	1

UNLESS OTHERWISE SPECIFIED:
DIMENSIONS ARE IN MILLIMETERS
SURFACE FINISH:
TOLERANCES:
LINEAR:
ANGULAR:

FINISH:

DEBURR AND BREAK SHARP EDGES

DO NOT SCALE DRAWING | REVISION

	NAME	SIGNATURE	DATE
DRAWN			
CHK'D			
APPV'D			
MFG			
Q.A			

TITLE:

MATERIAL:

DWG NO. PE pipes assem

A3

WEIGHT:

SCALE:1:20

SHEET 1 OF 1

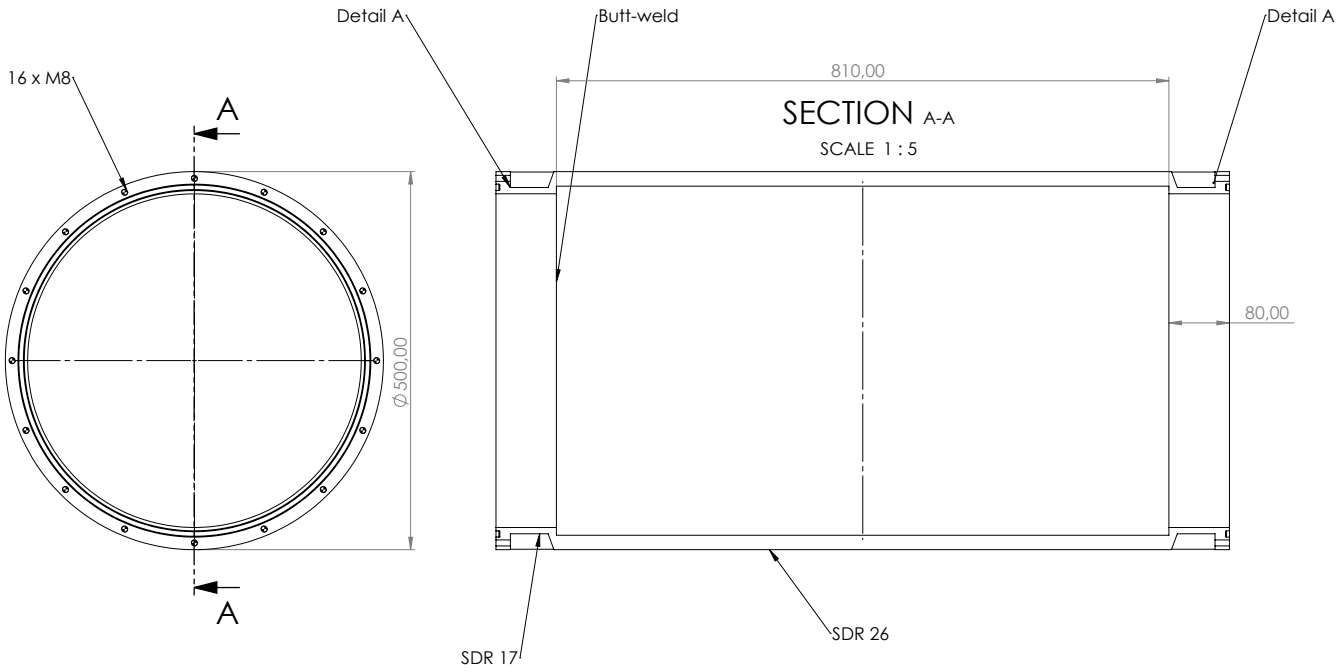

UNLESS OTHERWISE SPECIFIED: DIMENSIONS ARE IN MILLIMETERS SURFACE FINISH: TOLERANCES: LINEAR: ANGULAR:		FINISH:		DEBURR AND BREAK SHARP EDGES	DO NOT SCALE DRAWING	REVISION	
	NAME	SIGNATURE	DATE		TITLE:		
DRAWN	Almar						
CHK'D							
APP'V'D							
MFG							
Q.A				MATERIAL: PE-100	DWG NO. PE-front1		A3
				WEIGHT:	SCALE:1:10	SHEET 1 OF 1	

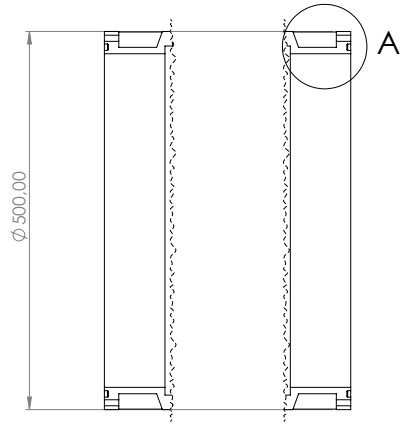

SECTION A-A

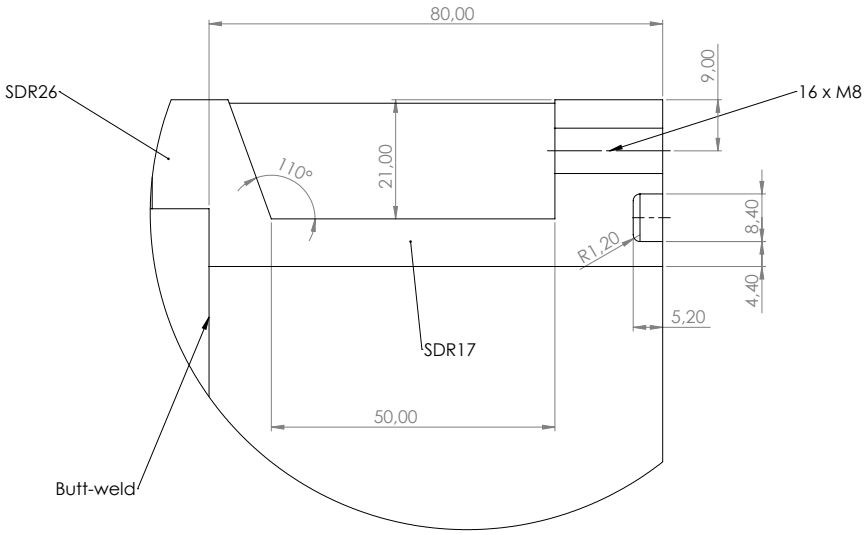

DETAIL A

SCALE 3 : 2

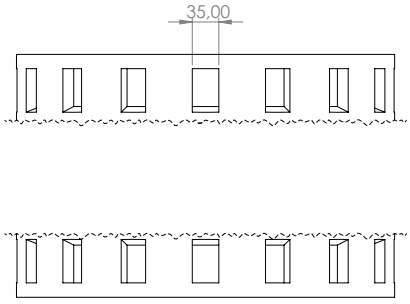

TOP VIEW

UNLESS OTHERWISE SPECIFIED: DIMENSIONS ARE IN MILLIMETERS SURFACE FINISH: TOLERANCES: LINEAR: ANGULAR:		FINISH:			DEBURR AND BREAK SHARP EDGES	DO NOT SCALE DRAWING	REVISION
	NAME	SIGNATURE	DATE			TITLE: Weld, bolt slot and O-ring groove detail	
DRAWN							
CHKD							
APPV'D							
MFG							
Q.A				MATERIAL:		DWG NO. Pe-pipe DETAIL A	A3
				WEIGHT:		SCALE:1:5	SHEET 1 OF 1

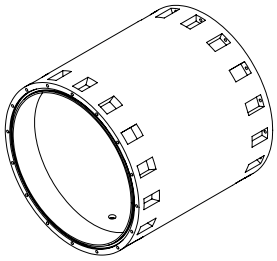

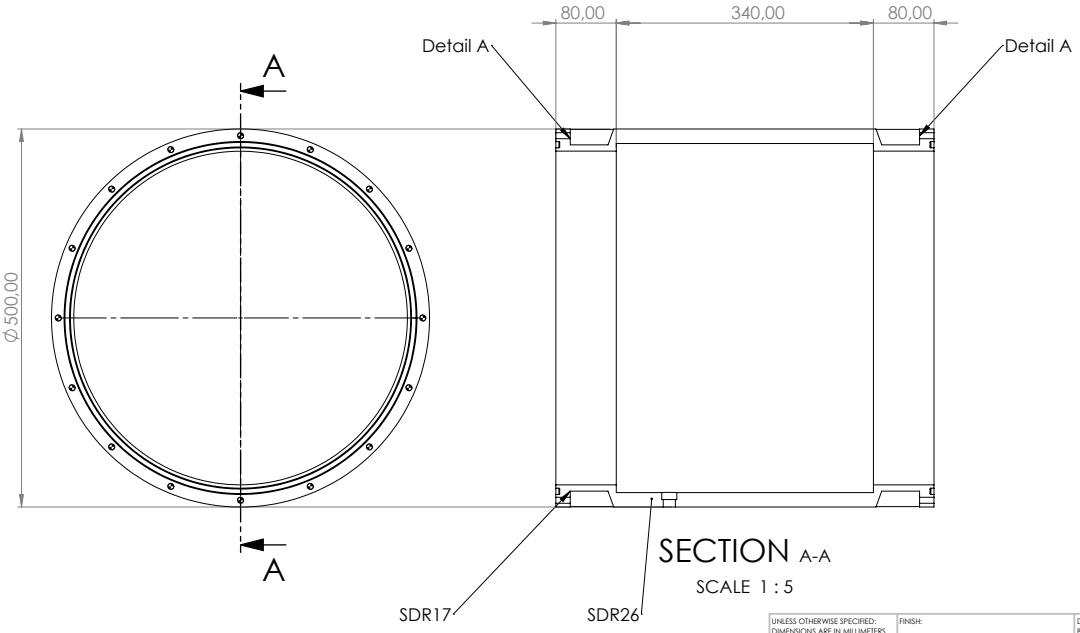

SECTION A-A

SCALE 1 : 5

UNLESS OTHERWISE SPECIFIED: DIMENSIONS ARE IN MILLIMETERS SURFACE FINISH: TOLERANCES: LINEAR: ANGULAR:			FINISH:			DEBURR AND BREAK SHARP EDGES	DO NOT SCALE DRAWING	REVISION
	NAME	SIGNATURE	DATE				TITLE:	
DRAWN								
CHKD								
APPV'D								
MFG								
Q.A				MATERIAL:			DWG NO. PE-rear-rudder	A3
				WEIGHT:			SCALE:1:10	SHEET 1 OF 1

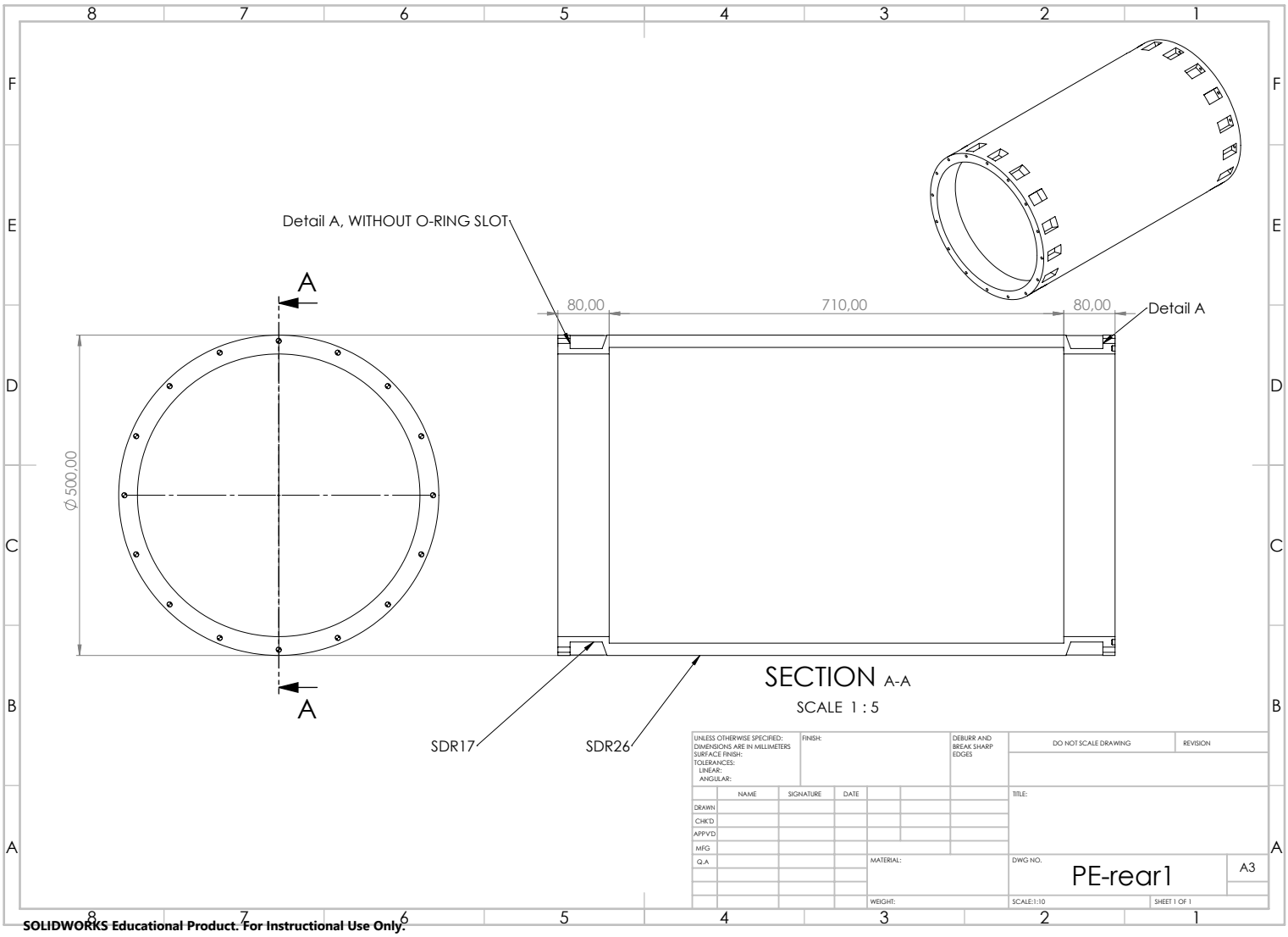

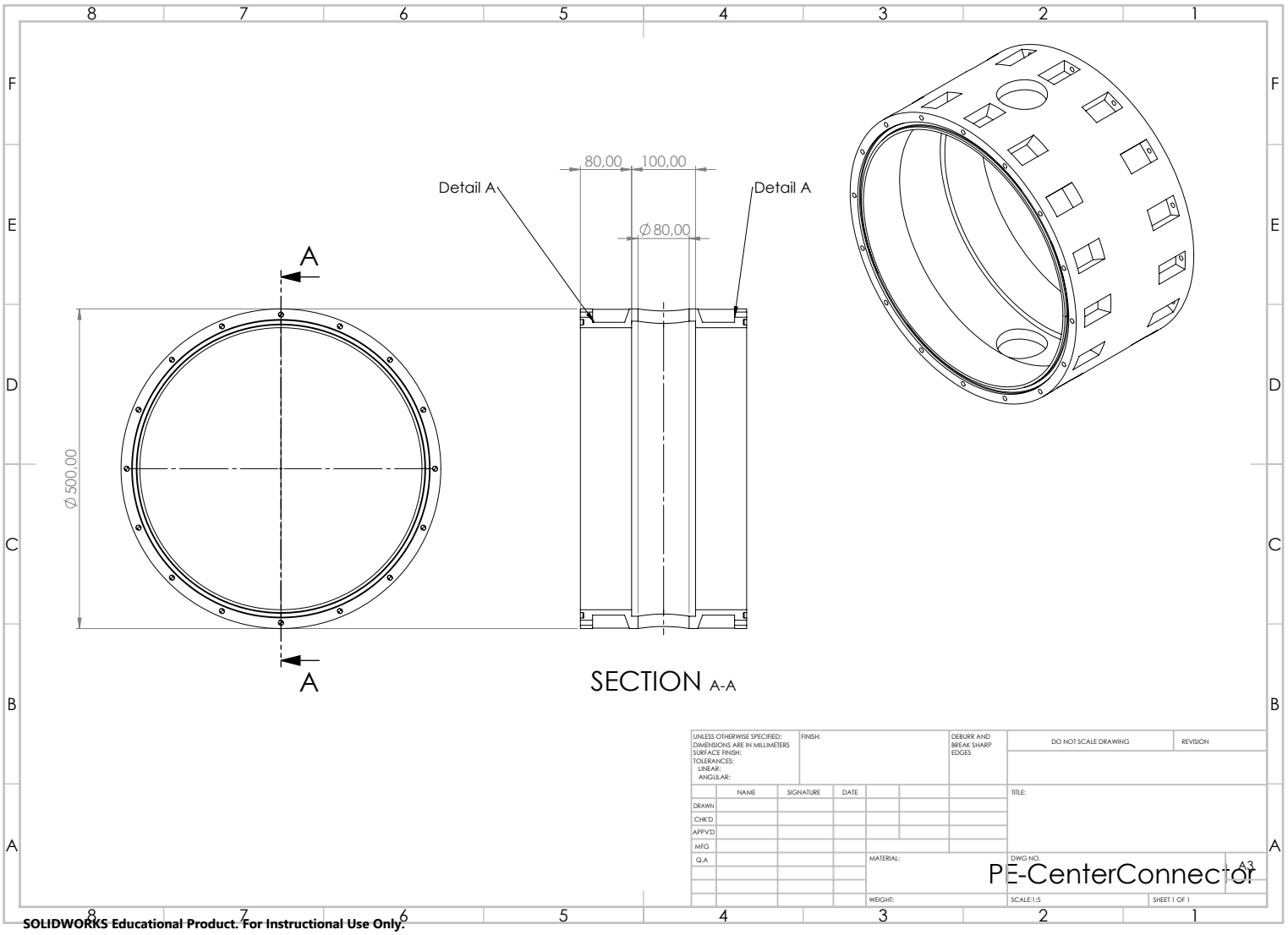

UNLESS OTHERWISE SPECIFIED: DIMENSIONS ARE IN MILLIMETERS SURFACE FINISH: TOLERANCES: LINEAR: ANGULAR:		FINISH:		DEBURR AND BREAK SHARP EDGES	DO NOT SCALE DRAWING	REVISION	
	NAME	SIGNATURE	DATE		TITLE:		
DRAWN							
CHKD							
APPV'D							
MFG							
Q.A							
				MATERIAL:	DWG NO. PE-CenterConnector		A3
				WEIGHT:	SCALE:1:5	SHEET 1 OF 1	

Appendix B

Relevant Data Sheets

TECHNICAL DATASHEET

SAP No. **30009055** **Article Description** **X-E-302g/m²-1270mm**

Textile Structure 7008669 **SAERTEX®**

ARTICLE CONSTRUCTION (in accordance with EN 13473-1)

Layer	Construction	Areal weight	Tolerance	Material
4	45 °	145 g/m²	+/- 5,0 %	E-glass 200 TEX
3	90 °	4 g/m²	+/- 5,0 %	E-glass 68 TEX
2	0 °	2 g/m²	+/- 5,0 %	E-glass 68 TEX
1	-45 °	145 g/m²	+/- 5,0 %	E-glass 200 TEX
Stitching		6 g/m²	+/- 1 g/m²	PES [Polyester] 76 dtex

Fiber input can be determined individually

FURTHER CHARACTERISTICS

Gauge	5,0	Stitching pattern	warp	Width (nominal)	1270 mm
Stitch length	3,00 mm	Total tolerance	+/- 5,2 %	Total areal weight	302 g/m²

Labelling (Standard) Every roll is equipped with a label in the core. A further label is located outside on the foil or on the box.

Packaging (Standard) Every roll is wound on a cardboard core and wrapped in foil. Further packaging options can be determined individually.

Storage With original packaging: No moisture recommendation and direct sunlight.
To avoid problems with humidity and electrostatic charge, fabrics to be conditioned 24 hours prior to processing, independent of storage conditions.

Fibre Specifics	EC9-33X1TEX	
Weave	2 x 2 Twill	

Weight and Dimensions

Thickness	0.2	mm
Width	1000	mm
Consolidated Thickness	0.2	mm
Areal Weight	200	g/m²

Product Data

Colour	White	
Format	Woven Fabric	
Fibre Type	Glass Fibre	

Mechanical Properties

Ends	13	/cm
Picks	13	cm

Compatible With

Compatible With	Epoxy	Yes
Compatible With	Polyester	Yes
Compatible With	Vinylester	Yes

General Properties

Gross Weight	0.2	kg

Figure B.1: [0/90] woven fabric data sheet.

Maricell

PVC ESPANSO RETICOLATO A CELLULE POLIEDRICHE CHIUSE - OUR KNOW HOW FOR OUR FOAM SINCE 1982

Maricell S.r.l. - via Villanova 15 I-32013 Longarone BL ITALIA - info@maricell.it - tel +39 0437 771577-772318 fax +39 0437 772059

Mycell

structural core foam

technical data sheet

Foam				M040	M048	M060	M080	M100	M130	M200	M250	H060	H080
Density	ASTM D1622	kg/m^3	nominal	40	48	60	80	100	130	200	250	60	80
			range	36 - 46	43 – 55	54 - 69	72 - 92	90 - 115	120 - 150	180 - 250	225 - 288	54 - 69	72 - 92
Compressive strength	ASTM D1621-10	MPa	average	0,51	0,69	0,96	1,43	1,93	2,73	4,84	6,56	0,90	1,46
			min-ave	*0,30*	*0,48*	*0,75*	*1,22*	*1,72*	*2,52*	*4,64*	*6,36*	*0,84*	*1,40*
			min-min	*0,20*	*0,37*	*0,61*	*1,03*	*1,47*	*2,25*	*4,00*	*5,47*	*0,67*	*1,17*
Compressive modulus	ASTM D1621-10	MPa	average	24	33	46	68	90	125	212	279	44	64
			min-ave	*10*	*18*	*31*	*53*	*76*	*111*	*198*	*264*	*39*	*59*
			min-min	*5*	*13*	*25*	*44*	*64*	*99*	*172*	*231*	*32*	*51*
Tensile strength	ASTM D1623	MPa	average	0,74	0,95	2,11	2,60	3,08	3,81	6,61	7,34	2,00	2,80
			min-ave	*0,47*	*0,66*	*1,33*	*1,82*	*2,31*	*3,04*	*5,61*	*6,32*	*1,87*	*2,67*
			min-min	-	-	*1,19*	*1,63*	*2,06*	*2,79*	*5,33*	*5,96*	*1,63*	*2,35*
Tensile modulus	ASTM D1623	MPa	average	74	87	106	137	169	216	415	480	101	142
			min-ave	*44*	*57*	*75*	*107*	*138*	*185*	*343*	*409*	*59*	*101*
			min-min	*36*	*49*	*66*	*94*	*123*	*170*	*317*	*376*	*47*	*85*
Shear strength	ASTM C273	MPa	average	0,41	0,55	0,77	1,13	1,49	2,03	3,59	4,67	0,78	1,16
			min-ave	*0,34*	*0,49*	*0,70*	*1,06*	*1,43*	*1,97*	*3,23*	*4,13*	*0,74*	*1,12*
			min-min	*0,25*	*0,40*	*0,60*	*0,92*	*1,25*	*1,79*	*2,81*	*3,79*	*0,63*	*0,97*
Shear modulus	ASTM C273	MPa	average	13	16	21	29	37	49	78	98	20	27
			min-ave	*9*	*12*	*17*	*25*	*33*	*45*	*74*	*94*	*19*	*26*
			min-min	*6*	*10*	*14*	*22*	*29*	*41*	*65*	*84*	*16*	*23*
Shear elongation at break	ASTM C273	%	average	5	9	13	20	25	32	41	40	27	27
Thermal conductivity at room temperature	ISO 8301	W/mK		0,031	0,031	0,031	0,033	0,035	0,039	0,048	0,050	0,031	0,036
Water absorption		%		1	1	1	1	1	1	1	1	1	1
Standard block dimensions		mm		1330 2850 84	1270 2730 80	1150 2450 78	1020 2180 72	950 2050 68	850 1900 58	750 1600 48	700 1500 47	1120 2400 78	1005 2150 75
Colour				azure	lilac	yellow	green	red	blue	hazel brow n	light green	pink	hazel brow n

Fire resistance DIN5510 S4 SR2 ST2 FED <1

The reported data, derived from laboratory tests for Type Certification.

No warranty is made on the basis of these data. Customers have to verify the data needed for the specific application, performing the necessary tests on the product.

No warranty is released for any particular application. Maricell may update the data of this report. Check the last version.

PRODUCT CONFIGURATION

Actuator LA33

Item No:
Item Name: 33150100000A3B1A=ACBC414200271
Protection Class: IP66
Load Type: Push
Load: 2250 N
Self Lock: 2250 N
Speed: 21,00 mm/s
Voltage: 24 V
Gear Ratio: 01:39
Brake: Yes
Platform: IC
IC Advanced
End-Stop Type: Signal Switch
Feedback : Hall Potentiometer 4 - 20mA
Endstop Signals Output : Yes
Stroke length: 100 mm.
Installation Dimension: 271 mm.
Colour: Dark Olivish Grey (NCS S7000-N)
Safety Nut: No
Piston Rod Eye: BallEye, ø10H7, Stainless Steel AISI304
Back Fixture: With Slot, ø12,2, Stainless Steel AISI 304,
Orientation: 0 degrees,
Power Cable:
Plug Type: OpenEnds
Cable Type: Straight 5000 mm.
Signal Cable:
Plug Type: OpenEnds
Cable Type: Straight 5000 mm.
Packing: Number LA33 on ½ pallet: 56 pcs.
Number LA33 on 1/1 pallet: 112 pcs.

LINAK®
WE IMPROVE YOUR LIFE

Almar Vreim Brandal

NTNU
Norwegian University of
Science and Technology